Molecular Neurobiology (2019) 56:2618–2639
https://doi.org/10.1007/s12035-018-1262-y

# The Role of Deimination in Regenerative Reprogramming of Neurons

Di Ding[1,2] · Mabel Enriquez-Algeciras[1,2] · Anddre Osmar Valdivia[1,2] · Juan Torres[1,2] · Cameron Pole[2] · John W Thompson[3] · Tsung-han Chou[1,2] · Miguel Perez-Pinzon[2,4] · Vittorio Porciatti[1,2] · Susan Udin[5] · Eric Nestler[6] · Sanjoy K. Bhattacharya[1,2]

Received: 22 May 2018 / Accepted: 17 July 2018 / Published online: 26 July 2018


## Abstract

Neurons from the adult central nervous system (CNS) demonstrate limited mRNA transport and localized protein synthesis versus developing neurons, correlating with lower regenerative capacity. We found that deimination (posttranslational conversion of protein-bound arginine into citrulline) undergoes upregulation during early neuronal development while declining to a low basal level in adults. This modification is associated with neuronal arborization from amphibians to mammals. The mRNA-binding proteins (ANP32a, REF), deiminated in neurons, have been implicated in local protein synthesis. Overexpression of the deiminating cytosolic enzyme peptidyl arginine deiminase 2 in nervous systems results in increased neuronal transport and neurite outgrowth. We further demonstrate that enriching deiminated proteins rescues transport deficiencies both in primary neurons and mouse optic nerve even in the presence of pharmacological transport blockers. We conclude that deimination promotes neuronal outgrowth via enhanced transport and local protein synthesis and represents a new avenue for neuronal regeneration in the adult CNS.

**Keywords** Deimination · Regeneration · Development · PAD2

## Introduction

The delivery of cargo to specific compartments within the neurons is critical for establishing unique cellular domains and plays a crucial role during development and synapse formation [1]. During these processes, local mRNA synthesis becomes a heavily regulated process mediated by motor, adaptor, and scaffolding proteins that regulate mRNA transport to specific compartments [1, 2]. Cargo destined for specific compartments is transported based upon the unique

**Electronic supplementary material** The online version of this article (https://doi.org/10.1007/s12035-018-1262-y) contains supplementary material, which is available to authorized users.

✉ Sanjoy K. Bhattacharya
sbhattacharya@med.miami.edu

Di Ding
DDing@med.miami.edu

Mabel Enriquez-Algeciras
malgeciras@med.miami.edu

Anddre Osmar Valdivia
Aov7@med.miami.edu

Juan Torres
jetch2011@gmail.com

Cameron Pole
cpole82190@gmail.com

John W Thompson
JThompson@med.miami.edu

Tsung-han Chou
TChou@med.miami.edu

Miguel Perez-Pinzon
perezpinzon@med.miami.edu

Vittorio Porciatti
VPorciatti@med.miami.edu

Susan Udin
susan.udin@gmail.com

Eric Nestler
eric.nestler@mssm.edu

Extended author information available on the last page of the article

association with compartment-specific motor complexes whose specific complexation occurs before axonal specification [2]. Hence, defects of motor proteins that are involved in this transport system have been demonstrated to be associated with neuronal degeneration [3–7]. The mammalian peripheral nervous system (PNS) maintains the ability to regenerate into adulthood [8–10], whereas neurons of the central nervous system (CNS) are incapable of regeneration [6, 11, 12]; therefore, the loss of regenerative capacity has been attributed to be the result of reduced levels of translational machinery and growth inhibitors that prevent protein synthesis following injury in the mature CNS [3, 6, 7, 13]. Compartmental local protein synthesis by means of RNA trafficking has been reported in dendrites in neuronal cultures [8], and several independent studies have now corroborated selective trafficking of mRNA and their local translation in specific neuronal compartments [9–12]. Despite these demonstrations, restoration of protein synthesis and transport in mature neurons that promote neuronal growth remains a challenge [3]. In addition, the mechanisms that promote neuronal transport through the selection of cargoes and their interactions with motor proteins (which lead to the distribution of mRNA and local proteins synthesis) remain poorly understood. Posttranslational modifications (PTMs) such as deimination (the conversion of protein-bound arginine into citrulline) are another layer of regulatory mechanisms that remains to be explored [14]. Due to the lack of a bona-fide reversal enzyme, deimination is considered to be an irreversible and long-term PTM whose longevity highlights its potential for long-term regulatory effects. Thus far, only a limited number of proteins have been identified to undergo deimination [15]; however, deimination is highly regulated in different cell types, and dysregulation of deimination has been reported in neurodegenerative diseases such as multiple sclerosis and glaucoma [16–18]. Here, we demonstrate that deimination regulates the interaction of cargo molecules and molecular motors, suggesting that neuronal transport affects neurite outgrowth and neuronal function in vitro and in vivo [11].

## Results

### Deimination Level Is Associated with Neuronal Outgrowth

Deimination has been observed in the infant CNS which showed higher levels of deimination when compared to adult brains [19]; in addition, deimination has been documented to decrease in aged rats when compared to young rats [20]. As deimination is under independent regulation in different cell types, the co-existence of hyperdeimination in astroglial cells and hypodeimination in neurons of neurodegenerative diseases with inflammation [21] makes it difficult to observe deimination changes when neurons undergo degeneration. We utilized three different systems, ocular rotation in frogs, cocaine treatment in mice, and neuronal cultures (in which the effects of deimination in glial cells are minimized), to analyze changes in neuron-specific deimination during neurite outgrowth and retraction. Ocular rotation in frogs results in new arborization (new neurite formation) in the optic tectum without activation of astroglial cells [22, 23], rendering it a suitable model for detection of deimination in neurons without interference from glial cells. Neurons undergoing arborization were traced by cholera toxin subunit B. Immunohistochemical (IHC) analysis showed a significant increase in deimination in the contralateral tectal lobes of the rotated eyes compared to controls (Fig. 1a, b), commensurated with increased neurite outgrowth that co-localizes with neural arborization as indicated by a tracer (Fig. 1a). These findings were further corroborated using Western blot analysis showing increased protein-bound citrulline (deimination) in the rotated eye of the contralateral tectal lobe (Fig. 1c). The increase in deimination was associated with increased expression of peptidyl arginine deiminase 2 (PAD2), the major cytoplasmic deiminase in neurons (Fig. 1c). Our second model was the chronic cocaine-treated mouse cerebellum, which undergoes degeneration and neurite retraction [24], with no reported astroglial cell activation. In contrast to the eye-rotated frog optic tectums, PAD2 levels in the cerebellums of chronic cocaine-treated mice (C57BL/6J) showed a significant decrease when compared to the saline-treated controls (Fig. 1d–f). The reduction in PAD2 correlates with reduced axonal marker SMI312 and the synaptosomal protein SNAP-25, suggesting rearrangement of neurons (Fig. 1d–f).

We further investigated deimination levels in primary rat neurons cultures and in established neuronal cell lines (PC12 and Neuro 2A) under neurite growth permissive and growth inhibitory conditions independently. PAD2 expression increased after 6 days in mouse primary neurons (E17) (Fig. 1g), commensurate with PAD2 mRNA increase during early development in the first week and decrease during adulthood (Fig. 1h). Nerve growth factor (NGF) was used to induce neurite growth in PC12 cells and primary neurons (Fig. 2a), while myelin basic protein (MBP) fragments were used as a growth inhibitor for Neuro 2A cells and primary neurons (Fig. 2b). As expected, PAD2 expression was up-regulated in NGF-treated cells but decreased in MBP-treated cells/neurons (Fig. 2a–c). These results suggest that deimination levels are associated with neurite outgrowth and retraction. Early steps of neuronal compartmentalization are associated with polarized cargo trafficking; therefore, subsequent experiments attempted to unravel the association between deimination and polarized trafficking.

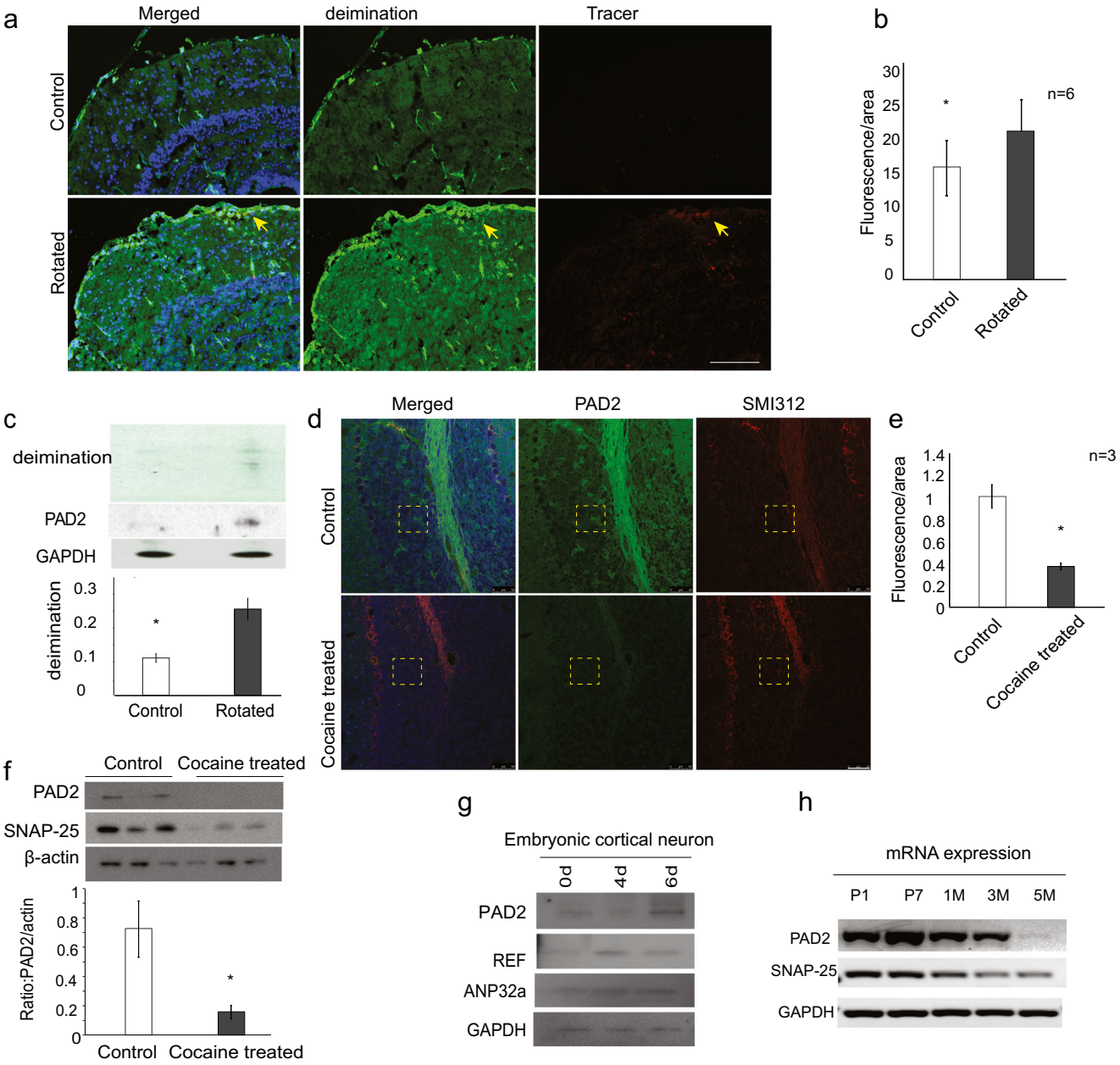


**Fig. 1** Deimination level is associated with growth status of neuron. **a** Representative normal and eye-rotated frog tectum, detected with antibody against deimination as indicated. Tracer indicates isthomotectal projection after eye rotation concomitant with elevated deimination. Bar = 50 μm. **b** Semiquantitative fluorescent signal from comparative area quantified by ImageJ ($n = 6$; $*p \leq 0.005$). **c** Representative Western blot analysis of deimination and PAD2 level in frog tectum (control and rotated as indicated). Densitometric quantification from similar blots ($n = 6$; $*p \leq 0.005$). **d** Representative saline (control) and cocaine-treated (chronic) mouse cerebellum, detected with anti-PAD2 and SMI312 antibody as indicated. Bar = 50 μm. **e** Fluorescent signal from comparative area quantified by ImageJ ($n = 3$; $*p \leq 0.005$). **f** Western blot analysis of SNAP-25 and PAD2 level in mouse cerebellum (control and chronic cocaine treatment as indicated). Densitometric quantification from similar blots ($n = 6$; $*p \leq 0.005$). **g** Western blot analysis of PAD2, REF, and ANP32a in 0-, 4-, and 6-day neurons; GAPDH is used as control. **h** Detection of PAD2 expression in postnatal day 1 and 7 (P1, P7), 1-, 3-, and 5-month-old mouse optic nerve

## Deimination Is Associated with Polarized Trafficking

Acidic nuclear phosphoprotein 32a (ANP32a) and RNA export factor (REF) are mRNA-binding proteins, primarily localized in the nucleus [25, 26], that are deiminated in neurons during normal conditions [18, 21], but show a decreased in deimination in neurodegenerative diseases [21]. ANP32a and REF play a role in mRNA processing/export and neuronal differentiation, respectively [27]. Deiminated REF facilitates the transport of mRNAs such as ATP5b and SNAP-25, resulting in their increased dendritic synthesis [18, 21]. Although PAD2 expression levels lack correlation with the

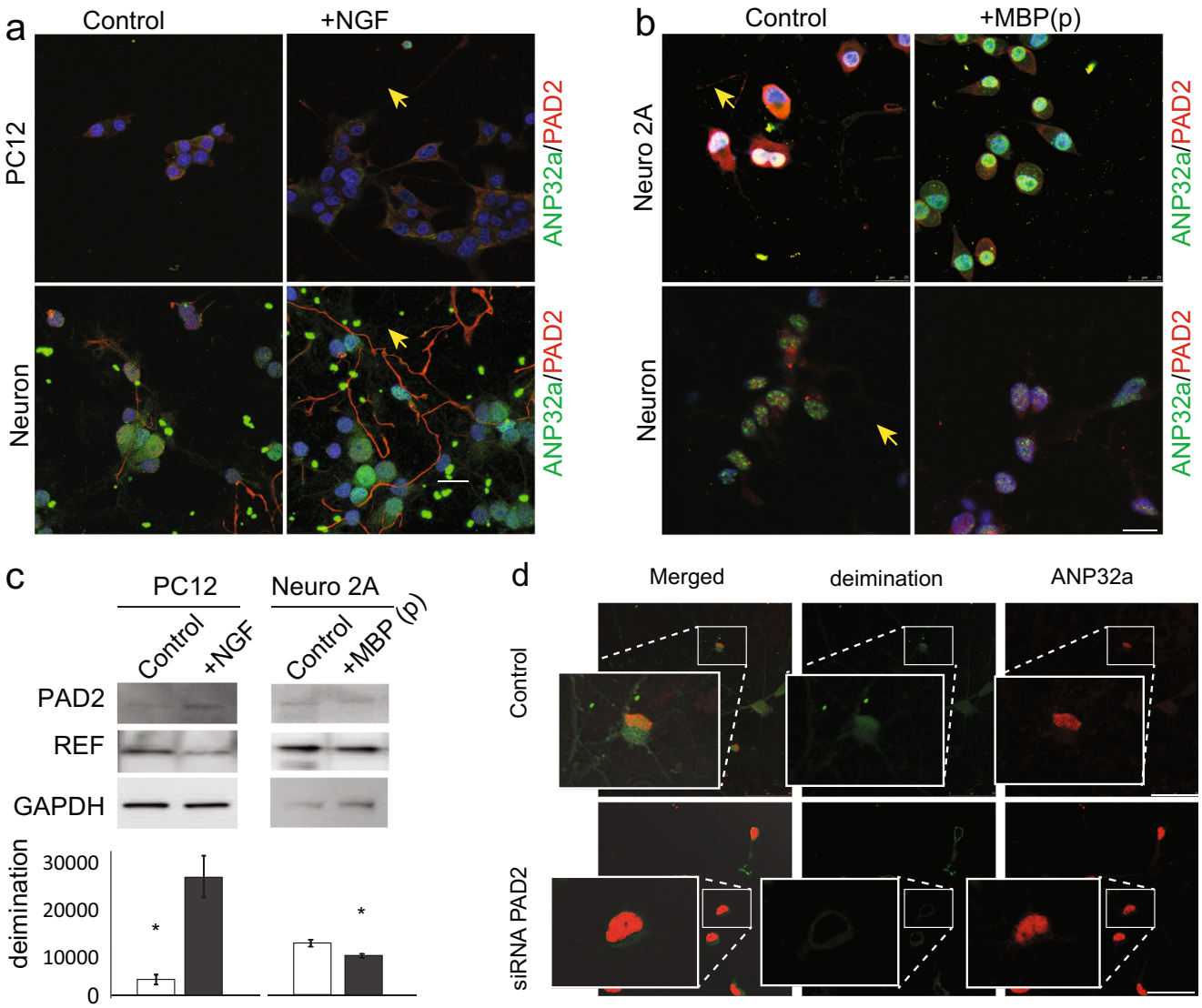


**Fig. 2** Deimination is associated with neuronal growth and polarity. **a**, **b** PAD2 expression by immunocytochemistry in two neuronal cell lines, PC12 and Neuro 2A. Bar = 20 μm. **a** Detection of PAD2 and ANP32a in PC12 cells and primary cortical neurons without (control) or with nerve growth factor (NGF). **b** Detection of PAD2 and ANP32a expression in Neuro 2A cells and primary cortical neurons without (control) or with a treatment of 20 aa inhibitory peptide of MBP (MBP P). **c** Western blot of PAD2, REF in PC12, and Neuro 2A cell lines as indicated. Densitometric quantification of deimination level from similar blots ($n = 6$; $^*p \leq 0.005$). **d** Detection of ANP32a location and deimination (green) in cortical neurons without (control) and with ANP32a (red) siRNA-mediated PAD2 inhibition

expression levels of REF and ANP32a (Figs. 1g and 2a–c), we found that ANP32a is transported in a polarized manner in neurons and consistently co-localizes with the deimination signal (Fig. 2d). Disruption of deimination by PAD2 knock-down with shRNA abolished ANP32a polarization (Fig. 2d), indicating a role of deimination in its transport.

## Proteins and Their Interactors Under Regulation of Deimination

REF and ANP32a were detected in the pool of PAD2 interactors by immunoprecipitation (IP) (Fig. 3a). In contrast, molecular motors dynactin (DCTN) and KIF21b were not deiminated and as such were not pulled down by PAD2. REF was found to associate with dynactin and kinesins (KIF21b and KIF5A) from reciprocal IPs with different motor proteins (Fig. 3b), indicating that PAD2 is likely indirectly interacting with motor proteins through REF. More extensive mass spectrometric analysis identified several PAD2 pulled down proteins that are related to ribonucleoproteins (RNPs) and RNA granules (Table 1), suggesting that PAD2 plays a role in the mechanism of mRNA transport.

To determine deiminated REF interactors, nondeiminated REF recombinant proteins were produced

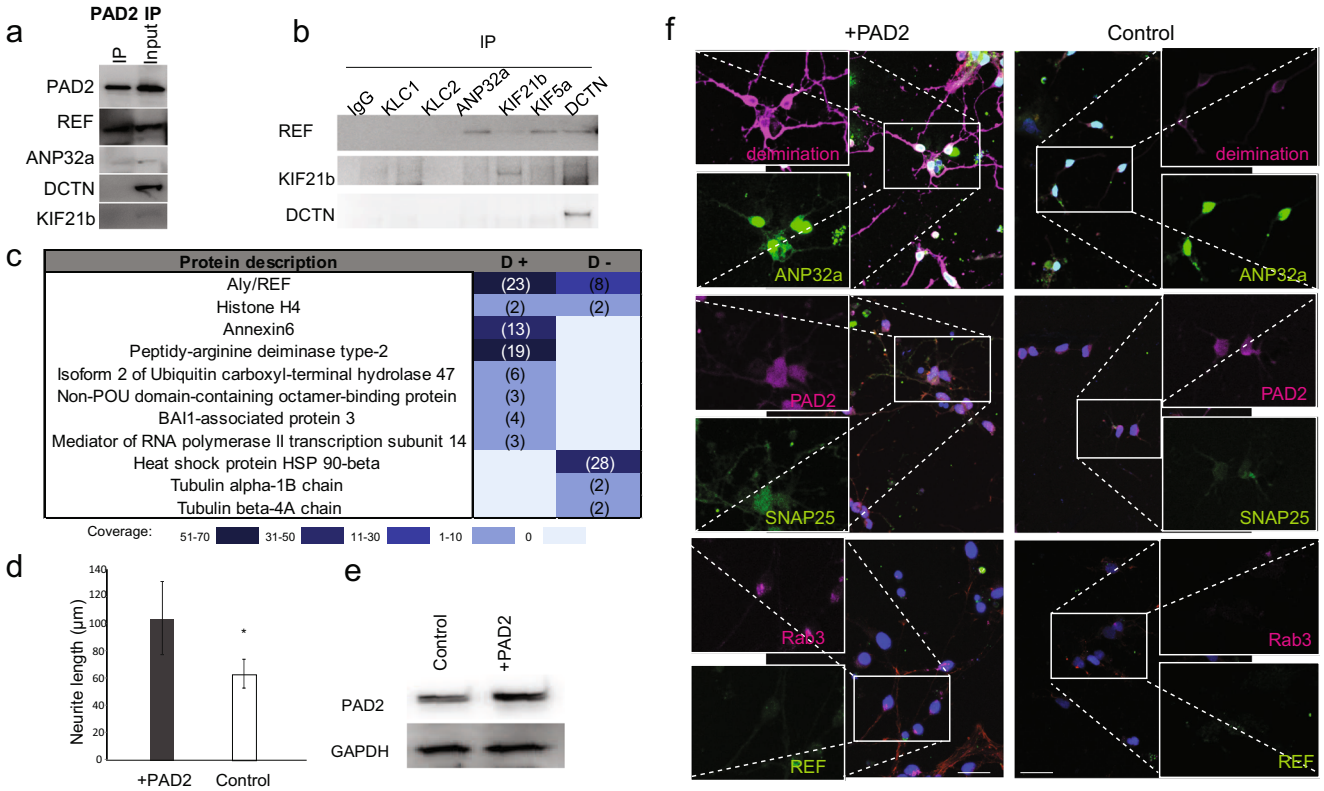


**Fig. 3** Proteins and their interactors under regulation of deimination. **a** Western blot of REF, ANP32a, dynactin (DCTN), and KIF21b in the immunoprecipitation (IP) products as indicated using PAD2 antibody in primary cortex cultures. **b** Western blot of REF, KIF21b, and DCTN in the IPs of different motor proteins. **c** Pulldown assay with mass spectrometry using nondeiminated REF (D−) and deiminated REF (D+). **d** Comparison of average neurite length for control and PAD2 overexpression as indicated ($n = 20$ neurons per group; $^*p \leq 0.005$). **e** Representative Western blot indicates posttransfection PAD2 expression. **f** Detection of ANP32a, PAD2, SNAP-25, and Rab3 in primary cortical neuron with overexpression of PAD2 and control (empty viral vector). Bar = 20 μm. Antibodies used in this study are listed in Online Resource 1

in *Escherichia coli* (lacks deiminase), and a fraction was in vitro deiminated by adding purified PAD2. Equal amounts of nondeiminated (control) and deiminated REF were used to pull down interactors in neuronal cells. Deiminated REF associated with different cohorts of RNA processing proteins (Fig. 3c), suggesting that deiminated REF may play a role as a specialized mRNA transporter that likely exhibits unique cargo selection depending on the cell compartment.

Increased PAD2 levels induced by viral vector expression in primary neurons promoted neurite elongation (Fig. 3d–f), upregulation, and accumulation of end products GTPase Rab3 and SNAP-25 proteins (Fig. 3f). Simultaneously, increased ANP32a was found in neurites but not within the cell bodies (Fig. 3d–f), which coincided with elevated arborization. In contrast, PAD2 knockdown showed a shift in distribution of SNAP-25, ANP32a, and dynein in the cell body and neurites (Fig. 3f). Taken together, these results suggest that deimination is involved in the regulation of trafficking of specific proteins. We next investigated transport of cargo via molecular motors.

## Association of Deiminated Molecules and PAD2 with Motors Systems

PAD2 expression is related to neuronal growth and associated with mRNA-binding proteins such as ANP32a and REF, which in turn facilitates interaction with motor proteins (such as KIF21b and KIF5A). We questioned whether the transport and localized translation in different neuronal compartments facilitated by ANP32a and REF are the intrinsic neurite/neuronal growth mechanisms. To address this, we tested whether there is a shift in subcellular localization of specific mRNAs or proteins, or an overall increase in their levels with regulation of PAD2 expression. We utilized novel neuronal fractionation for compartmental level analyses. Laser capture microdissection (on unfixed tissues to preserve proteins) suitable to fractionate different compartments of neurons generated insufficient quantities of reproducible material to perform multiple biochemical analyses in our repeated trials. Therefore, we developed a new fractionation method using biotin-conjugated lectins (proteins that bind to sugars on cell

**Table 1** Selected interactors of PAD2

| Function/classification | Protein name | Accession | Species | Unique peptide | Peptide number | Peptide |
|---|---|---|---|---|---|---|
| Selected proteins from IP_PAD2 | | | | | | |
| | Protein-arginine deiminase type-2 | Q9Y2J8 | Human | 10 | 11 | ILSNESLVQENLYFQR, ILIGSSFPLSGGR, ELGLTEQDIIDLPALFK, GFPVVLDSPR, DGEAEEVATNGK, ELLGPDFGYVTR, WIQDEIEFGYIEAPHK, WLLSPSTTLR, YIHILGR, ETPWLPK, EPLFESVTSLDSFGNLEVSPPVTVNGK |
| Cytoskeleton | F-actin-capping protein subunit alpha-1 | P47753 | Mouse | 3 | 4 | IQVHYYEDGNVQLVSHK, DVQDSVTVSNEVQTTK, FITHAPPGEFNEVFNDVR, EASDPQPEDVDGGLK |
| | F-actin-capping protein subunit alpha-2 | P47754 | Mouse | 4 | 5 | DIQDSLTVSNEVQTAK, IEGYEDQVLITEHGDLGNGK, FTVTPSTTQVVGILK, IQVHYYEDGNVQLVSHK, FIIHAPPGEFNEVFNDVR |
| | Microtubule-associated protein 1B | P14873 | Mouse | 7 | 8 | SSYYVVSGNDPAAEEPSR, DIKPQLELIEDEEK, TTEAAATAVGTAATTAAVVAAAGIAASGPVK, TPGDFNYAYQKPENAAGSPDEEDYDYESQEK, TPEEGGYSYEISEK, AVLDALLEGK, DLTGQVPTPPVK, SSYYVVSGNDPAAEEPSRAVLDALLEGK |
| | Dynactin subunit 2 | Q6AYH5 | Rat | 1 | 1 | LLGPDAAINLADPDGALAK |
| | Tubulin beta-2A chain | Q13885 | Human | 1 | 8 | FPGQLNADLR, GHYTEGAELVDSVLDVVR, NSSYFVEWIPNNVK, EVDEQMLNVQNK, SGPFGQIFRPDNFVFGQSGAGNNWAK, ALTVPELTQQMFDSK, IREEYPDR, FWEVISDEHGIDPTGSYHGDSDLQLER |
| Eukaryotic translation | Eukaryotic translation initiation factor 3 subunit G | Q9Z1D1 | Mouse | 3 | 3 | ELAEQLGLSTGEK, EKLPGELEPVQAAQSK, GFAFISFHR |
| | Eukaryotic translation initiation factor 3 subunit B | Q4G061 | Rat | 3 | 3 | IINDYYPEEDGK, GTQGVVTNFEIFR, ETIIAFAWEPNGSK |
| | Eukaryotic translation initiation factor 4B | Q8BGD9 | mouse | 19 | 19 | VAAVQPPEEGPSR, SPPYTAFLGNLPYDVTEDSIK, AASIFGGAKPVDTAAR, ARPTTDSFDDYPPR, IRVDVADQAQDKDR, IRVDVADQAQDK, VDVADQAQDKDR, VDVADQAQDK, GDDSFGDKYR, DSDKTDTDWR, RGDDSFGDKYR, QLDEPKLDR, VDVADQAQDKDRDDR, SPPYTAFLGNLPYDVTEDSIKDFFR, VAAVQPPEEGPSRK, NRDSDKTDTDWR, SLENETLNK, GLNISAVR, SILPTAPR |
| Formation of ribosome | 40S ribosomal protein S14 | P13471 | Rat | 1 | 3 | IEDVTPIPSDSTR, TPGPGAQSALR, ELGITALHIK |
| | 60S ribosomal protein L13 | P41123 | Rat | 2 | 2 | STESLQANVQR, VDTWFNQPAR |
| | 60S ribosomal protein L14 | Q9CR57 | Mouse | 2 | 2 | LVAIVDVIDQNR, AAIAAAAAAAAAAK |
| | 60S ribosomal protein L28 | P41105 | Mouse | 1 | 1 | TVGVEPAADGK |
| | 60S ribosomal protein L4 | Q9D8E6 | Mouse | 2 | 3 | NIPGITLLNVSK, APIRPDIVNFVHTNLR, IEEVPELPLVVEDK |
| | 60S ribosomal protein L6 | P47911 | Mouse | 1 | 1 | SSITPGTVLIILTGR |
| Metabolism of protein | Caspase-9 | Q8C3Q9 | Mouse | 1 | 1 | DQARQLVTDLETRGR |
| Metabolism of mRNA | Putative RNA-binding protein 3 | O89086 | Mouse | 1 | 1 | YDSRPGGYGYGYGR |
| | Polyadenylate-binding protein 1-like | Q4VXU2 | Human | 1 | 2 | FSPAGPILSIR, AILTNQYMQRLSTMR |
| | THO complex subunit 4 | O08583 | Mouse | 2 | 2 | QQLSAEELDAQLDAYNAR, SLGTADVHFER |
| | Ubiquitin-like protein 4A | P21126 | Mouse | 1 | 1 | LVDSPATPIWQLISK |

surface proteins). We found two plant lectins [*Canavalia ensiformis* (designated as lectin 2) and *Maclura pomifera* (lectin 3)], that preferentially associated with neurites and the neuronal cell body, respectively (Fig. 4a). The lectin-bound neurons incubated with streptavidin-coupled magnetic beads allowed fractionation of neuronal compartments (described in the "Materials and Methods"). The eluents from purification steps were loaded onto a gel and their cellular compartmental location was determined by the markers Tau1 and GAPDH (Fig. 4a). The purity of the fractions was further evaluated by probing the blots for the cytoplasmic GAPDH and the synaptic marker SNAP-25. This approach allowed detection of the compartmental locations of PAD2 and ANP32/REF. The majority of REF was located within the neurites rather than the cell body (Fig. 4b). KIF21b was mainly localized to neurites, while dynactin was ubiquitous throughout both fractions (Fig. 4b). Increased PAD2 expression results in increased SNAP-25 and dynein levels and a shift in dynein localization from the cell body to neurites—an opposite effect from that observed when PAD2 expression was inhibited (Fig. 4c). We further determined if REF or ANP32a had a unique subset of interactors in different neuronal fractions using IP-mass spectrometry (Table 2). Some interactors are parts of RNP or RNA granules, both of which are enriched in neurites. We determined whether there are any differences between REF/ANP32a (both RNA-binding proteins) and the associated repertoire of mRNA in neurites and cell bodies of the neuron (Fig. 4d). ANP32a had a higher affinity for most mRNA in the cell body. However, REF had higher affinities for Sphk2 (Sphingosine Kinase 2) and Capza2 (F-Actin Capping Protein Alpha-2 Subunit)

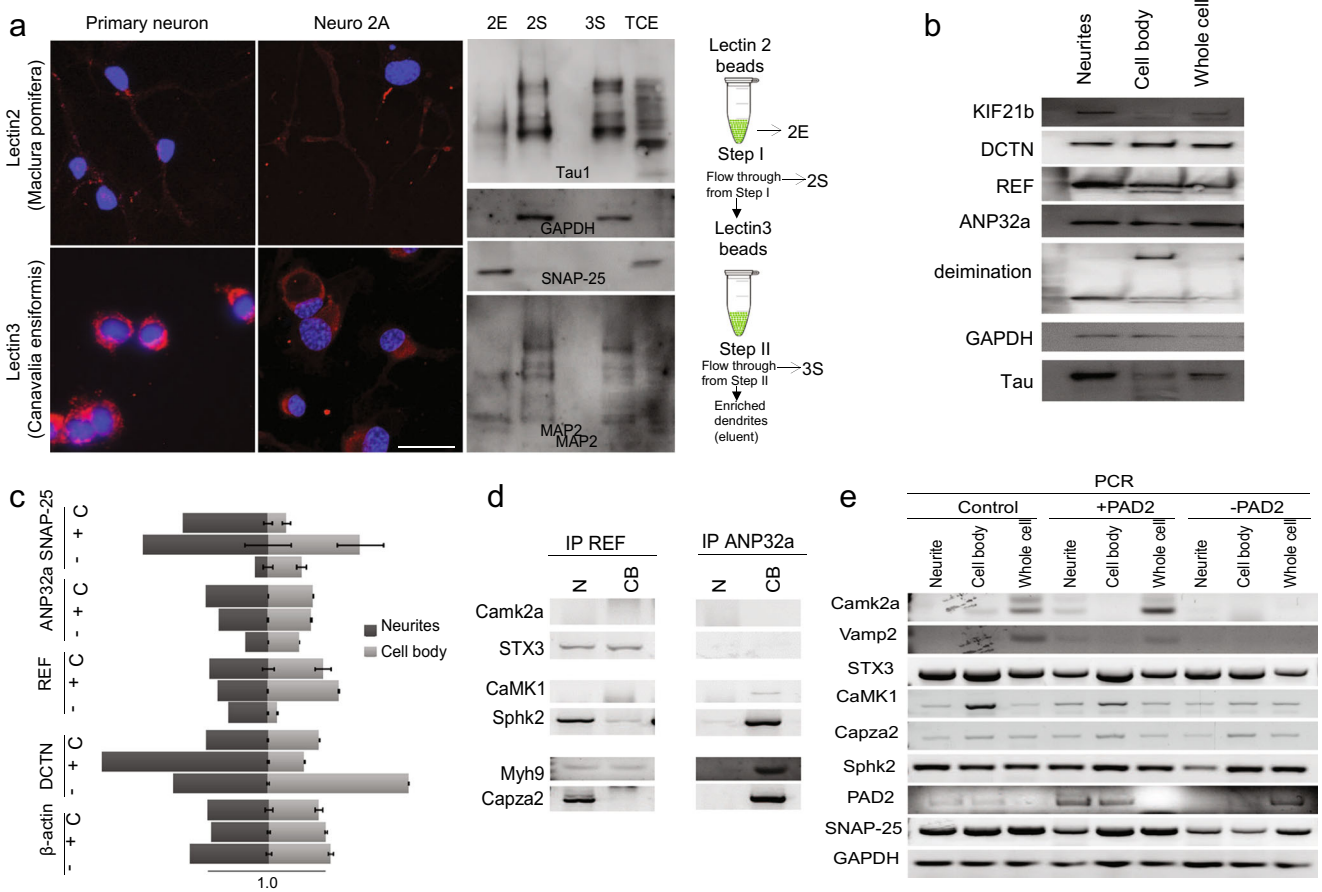


**Fig. 4** Deimination regulates cargo distribution in different compartments in neurons. **a** Localization of lectin 2 (*Maclura pomifera* lectin) and lectin 3 (*Canavalia ensiformis* lectin) in primary cortical neurons (IHC) and Neuro 2A cells as indicated. Bar = 20 μm. Western blot of fractions (illustrated with fraction-nomenclature in the schematic shown in the right) using markers for cell body and neurites from different eluents: 2E, eluent after lectin 2 binding; 2S, flow through after lectin 2 binding; 3S, flow through after lectin 3; TCE, total cell extract. **b** Western blot of selected proteins in different neuron compartmental fractions as indicated. **c** Quantification of distribution of selected proteins after induction (+) or inhibition (−) of PAD2 expression and controls (C) based on Western blot analysis ($n = 10$) and densitometry. Mean ± standard deviation. Neurite and cell body are color coded as indicated. **d** Selected mRNAs in cDNA derived from two independent immunoprecipitation (IP) products (using antibodies to REF and ANP32 as indicated). N, neurites; CB, cell body. **e** Distribution of select mRNAs in different cellular compartments of neurons after viral vector-mediated up- (+PAD2) or downregulation of PAD2 (−PAD2). The primers used in this study are listed in Online Resource 2

**Table 2** Different interactors associated with REF/ANP32a in different cell compartments

| Protein name | Accession | Species | Peptide number | Unique peptide | Peptide |
|---|---|---|---|---|---|
| Selected proteins from IP_ANP32 neurites | | | | | |
| 60S ribosomal protein L13 | P47963 | Mouse | 2 | 1 | STESLQANVQR, IAPRPASGPIRPIVR |
| 60S ribosomal protein L13a | P19253 | Mouse | 3 | 1 | KVVVVRCEGINISGNFYR, RGQAALER, VVVVRCEGINISGNFYR |
| 60S ribosomal protein L15 | Q9CZM2 | Mouse | 2 | 1 | SLQSVAEER, VLNSYWVGEDSTYKFFEVILIDPFHKAIR |
| 60S ribosomal protein L18 | P35980 | Mouse | 3 | 1 | GTVLLSGPR, TNRPPLSLSRMIR, TAVVVGTVTDDVR |
| 60S ribosomal protein L31 | Q1KSC7; P62900 | | 1 | 1 | SAINEVVTR |
| Heat shock cognate 71 kDa protein | P63017 | Mouse | 3 | 2 | TTPSYVAFTDTER, FEELNADLFR, DAGTIAGLNVLR |
| Tubulin alpha-1C chain | P68365; P68373 | Mouse | 8 | 6 | TIGGGDDSFNTFFSETGAGK, AVFVDLEPTVIDEVR, LISQIVSSITASLR, EIIDLVLDR, DVNAAIATIK, FDGALNVDLTEFQTNLVPYPR, LSVDYGK, EDMAALEK |
| Tubulin beta-3 chain | Q9ERD7 | Mouse | 5 | 2 | FPGQLNADLR, AILVDLEPGTMDSVR, YLTVATVFR, ALTVPELTQQMFDAK, MSMKEVDEQMLAIQSKNSSYFVEWIPNNVK |
| Tubulin beta-4B chain | P68372 | Mouse | 5 | 1 | FPGQLNADLR, EVDEQMLNVQNK, ALTVPELTQQMFDAK, IREEYPDR, MSATFIGNSTAIQELFK |
| Selected proteins from IP_ANP32 cell body | | | | | |
| Tubulin beta-2B chain | Q9CWF2 | Mouse | 12 | 4 | GHYTEGAELVDSVLDVVR, AILVDLEPGTMDSVR, ISEQFTAMFR, FPGQLNADLR, MSATFIGNSTAIQELFK, ALTVPELTQQMFDSK, IREEYPDR, EVDEQMLNVQNK, LHFFMPGFAPLTSR, YLTVAAIFR, INVYYNEATGNK, NSSYFVEWIPNNVK, ISEQFTAMFR |
| Tubulin beta-3 chain | Q9ERD7 | Mouse | 12 | 6 | GHYTEGAELVDSVLDVVR, AILVDLEPGTMDSVR, ISEQFTAMFR, FPGQLNADLR, IMNTFSVVPSPK, ALTVPELTQQMFDAK, YLTVATVFR, EVDEQMLAIQSK, ISVYYNEASSHK, NSSYFVEWIPNNVK, MSSTFIGNSTAIQELFK, VREEYPDR |
| Ubiquitin-40S ribosomal protein S27a | P62983 | Mouse | 2 | 1 | ECPSDECGAGVFMGSHFDR, TITLEVEPSDTIENVKAK |
| 40S ribosomal protein S6 | P62754 | Mouse | 1 | 1 | IPDWFLNR |
| 60S ribosomal protein L19 | P84099 | Mouse | 2 | 1 | STESLQANVQR, VDTWFNQPARK |
| 60S ribosomal protein L18 | P12001 | Rat | 2 | 2 | TAVVVGTITDDVR, GTVLLSGPR |
| 60S ribosomal protein L13 | P47963 | Mouse | 2 | 1 | LLADQAEAR, DGLIIRKPVTVHSR |
| Heat shock 70 kDa protein 1-like | P16627 | Mouse | 3 | 2 | TTPSYVAFTDTER, VEIIANDQGNR, TLSSSTQANLEIDSLYEGIDFYTSITRAR |
| 40S ribosomal protein S18 | P62270 | Mouse | 1 | 1 | LIEVDDER |
| Heat shock protein HSP 90-beta | P11499 | Mouse | 2 | 1 | GVVDSEDLPLNISR, YIDQEELNK |
| mRNA export factor | Q8C570 | Mouse | 1 | 1 | NAAEELKPR |
| E3 ubiquitin-protein ligase UBR5 | Q80TP3 | Mouse | 6 | 1 | NSLEDLTAEDFR, SSAGARDSRR, SRSVIIRELQR, VDGAYVAVK, NRGERDR, SLRLREMMR |
| Selected proteins from IP_REF neurites | | | | | |
| E3 ubiquitin-protein ligase XIAP | Q60989 | Mouse | 2 | 1 | NPFAPDRPPETHADYLLR, RISPNCR |

**Table 2** (continued)

| Protein name | Accession | Species | Peptide number | Unique peptide | Peptide |
|---|---|---|---|---|---|
| Tubulin alpha-1A chain | P68362; P68369 | Mouse | 5 | 1 | AVFVDLEPTVIDEVR, EIIDLVLDR, DVNAAIATIK, LIGQIVSSITASLR, NLDIERPTYTNLNR |
| Tubulin alpha-1C chain | P68365; P68373 | Mouse | 5 | 1 | AVFVDLEPTVIDEVR, EIIDLVLDR, LISQIVSSITASLR, DVNAAIATIK, NLDIERPTYTNLNR |
| Tubulin beta-2A chain | Q7TMM9 | Mouse | 6 | 5 | AILVDLEPGTMDSVR, FPGQLNADLR, EVDEQMLNVQNK, YLTVAAIFR, GHYTEGAELVDSVLDVVR, IREEYPDR |
| Selected proteins from IP_REF cell body | | | | | |
| 40S ribosomal protein S13 | P62301 | Mouse | 1 | 1 | GLSQSALPYR |
| 40S ribosomal protein S15a | P62245 | Mouse | 1 | 1 | MNVLADALK |
| 40S ribosomal protein S18 | P62270 | Mouse | 1 | 1 | IPDWFLNR |
| 40S ribosomal protein S3 | P62908 | Mouse | 3 | 1 | TPVEPEVAIHR, TPCGEGSKTWDRFQMR, SLEKVCADLIR |
| 60S ribosomal protein L13 | P47963 | Mouse | 2 | 2 | STESLQANVQR, GFSLEELR |
| 60S ribosomal protein L27 | P61358 | Mouse | 1 | 1 | YSVDIPLDK |
| 60S ribosomal protein L6 | P47911 | Mouse | 1 | 1 | YYPTEDVPR |
| 60S ribosomal protein L7a | P12970 | Mouse | 4 | 1 | VPPAINQFTQALDR, TCTTVAFTQVNSEDKGALAK, VVNPLFEKRPK, YDEIRRHWGGNVLGPK |
| Heat shock-related 70 kDa protein 2 | P17156 | Mouse | 1 | 1 | TTPSYVAFTDTER |
| Tubulin alpha-1A chain | P68362; P68369 | Mouse | 2 | 2 | LIGQIVSSITASLR, DVNAAIATIK |
| Tubulin beta-2B chain | Q9CWF2 | Mouse | 9 | 8 | GHYTEGAELVDSVLDVVR, AILVDLEPGTMDSVR, FPGQLNADLR, LAVNMVPFPR, LHFFMPGFAPLTSR, INVYYNEATGNK, EVDEQMLNVQNK, IREEYPDR, ISEQFTAMFR |
| Caspase-9 | Q8C3Q9 | Mouse | 1 | 1 | DQARQLVTDLETRGR |
| Elongation factor 1-alpha 1 | P62629; P10126 | Mouse | 7 | 2 | STTTGHLIYK, LPLQDVYK, THINIVVIGHVDSGK, EHALLAYTLGVK, QLIVGVNK, STTTGHLIYKCGGIDK, EAAEMGKGSFK |

mRNAs in the neurites than in other compartments, indicating that REF transport would change the distribution for these mRNAs. Whether deimination would affect the distribution of the selected mRNA was tested by overexpressing and knocking down PAD2 expression. As expected, mRNAs such as Camk2a, STX3, CaMK1, and Capza1 had different distributions between cell body and neurites when the level of deimination changed (Fig. 4e). These differences could be regulated by the transport of either REF or ANP32a. It has been established that distribution of STX3 and several other mRNAs is regulated through their untranslated (UTR) regions by RNA-binding proteins [21, 28, 29]. To study transport and translation, we developed a hybrid construct that has 5′ and 3′ UTR regions of STX3 and mCherry and a construct of REF fused with GFP (see "Materials and Methods" for details). In cortical neurons that were co-infected with virus containing the two constructs, STX3 and REF co-localized in the axons (Fig. 5b, bottom panels). In order to observe the translation of STX3, STX3-mCherry signals (Fig. 5b, top panels) were bleached at wavelength 546, where REF signal stays unaffected (Fig. 5b, middle panels). During the 4-min recovery time, mCherry (STX3 UTR) with REF signal perfectly co-localized and moved toward the axon, suggesting that REF is associated with STX3 during transport and translation. In comparison with neurons without REF overexpression, STX3 proteins took longer time to recover after bleaching, indicating that REF plays a role in transport and translation (Fig. 5a). In summary, these results suggest that PAD2 regulates mRNAs transport and protein translation through modification of REF and ANP32a. Moreover, their locations within neuronal compartments were found to be closely related to their deimination level.

Next, we questioned how PAD2 would affect neuronal transport, which required a model system for direct visualization of motor transport. In order to label live neurons without disrupting their activity, we looked at small molecules that specifically interact with motor proteins and can be easily introduced into the cell. For this application, lipid molecules are ideal candidates (Fig. 6a), and some lipids showed specificity to the motor systems (Fig. 6b). To identify the lipids that associate with different motors, we performed IPs against different motor proteins followed by lipid identification from the eluent (Fig. 6c). This approach identified several lipids which were motor specific, such as binding to KIF21b but not KIF5a, allowing to distinguish between anterograde and retrograde transport. A custom fluorescent lipid probe was designed from one of the candidates (a glycolipid, FMC-5(d18:1/20:0)), synthesized commercially, and tested on neurons. There was a time-dependent decrease in axonal fluorescence, suggesting that this lipid was associated with retrograde transport in contrast to a control (phosphatidylserine) lipid (Fig. 6a). We used this approach to further evaluate the effects of deimination on neuronal transport. Primary neurons (E17), grown in an axon isolation chamber [27] (that contains microgrooves to guide neurite growth), were subjected to elevation in deimination by viral vector-mediated PAD2 expression. Two neuronal transport blockers (lidocaine and vincristine) were used to interrupt neuronal transport concurrent with overexpressed PAD2 or control [30, 31]. Fluorescent lipid probes were detected using live imaging. As shown in Fig. 6d, e (Movies 1 and 2), transport in the control cells

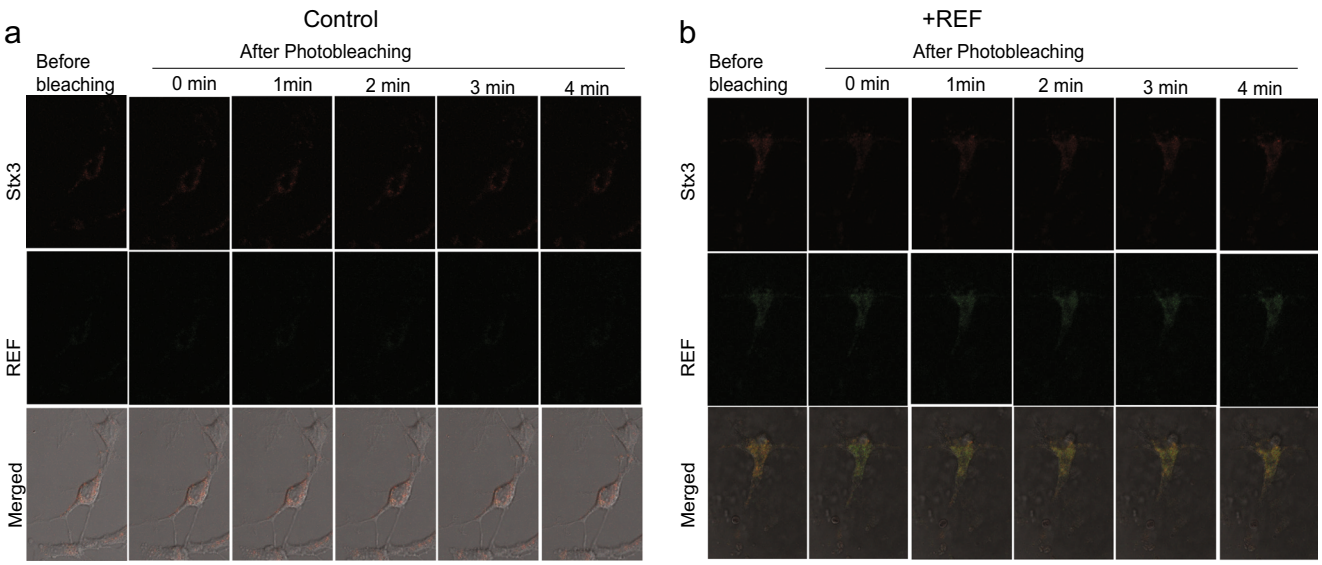


**Fig. 5** REF regulated mRNA transport and translation. The recovery of fluorescent signals after bleaching was monitored from 0 s to 4 min with 1 min interval between control (**a**) and the cells with overexpression of REF (**b**). The red signal is from a construct that expresses mCherry protein flanked with 5′ and 3′ untranslated region (UTR) of STX3. The green signal is from REF fused with GFP. The REF binding (with UTR regions of STX3) and translation of this construct results in mCherry expression. Arrows indicate co-localization

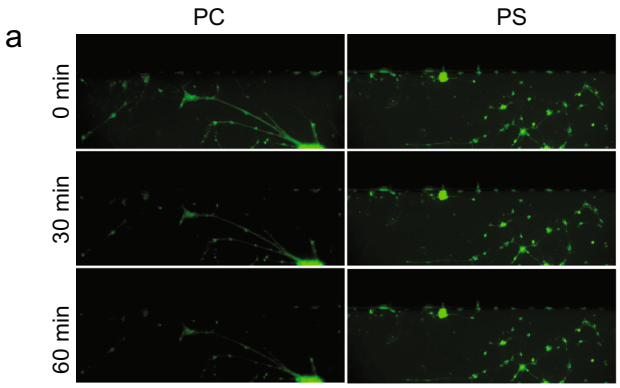


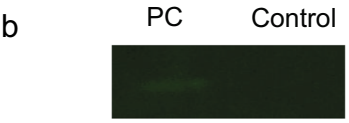


| Mass Spec | | |
|---|---|---|
| Accession No. | Protein | Peptide |
| P15205 | Microtubule-associated protein 1B | 1 |
| P38650 | Cytoplasmic dynein 1 heavy chain 1 | 3 |
| P48975 | Actin, cytoplasmic 1 | 6 |

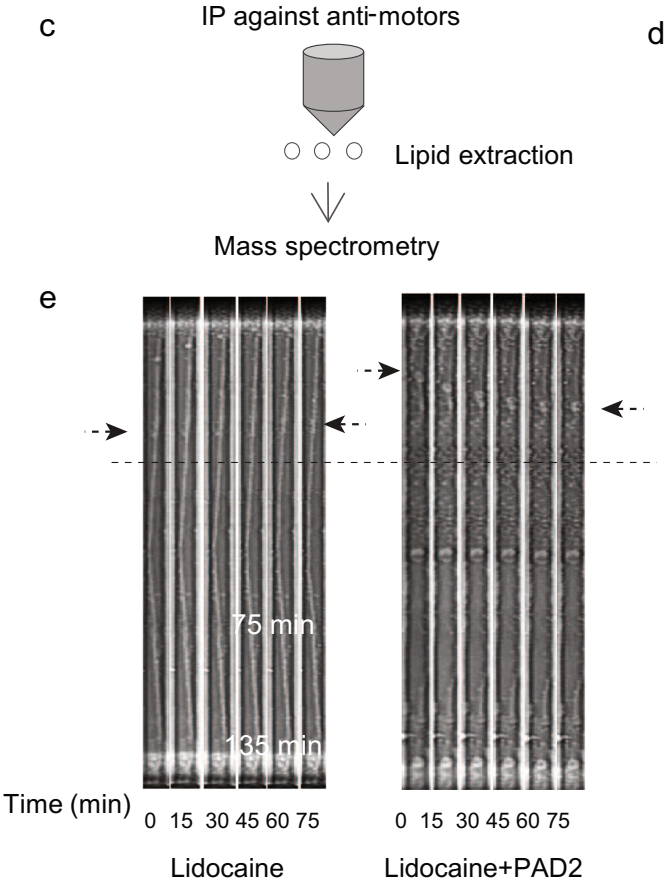


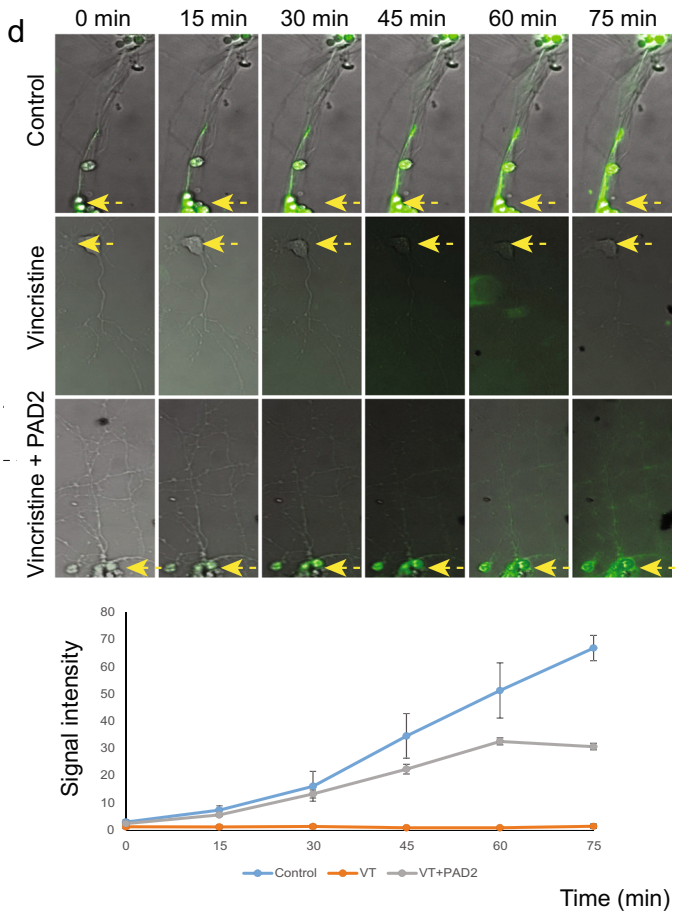


**Fig. 6** Deimination and neuronal transport probed using fluorescent lipid tracers. **a** Fluorescent lipid transport in neurons. Transport of phosphatidylcholine (PC) and phosphatidylserine (PS) is as indicated. **b** Fluorescent image of PHAST gel fractionated neuronal extract cross-linked with lipid (PC), and the proteins from the bands were extracted, followed by mass spectrometry. The control refers to a PS lipid cross-linked neuronal extract proteins. **c** Scheme for lipid identification. Anti-motor IP products are subjected to lipid extraction and mass spectrometry. **d** Quantification of fluorescent lipid signal. Blue, red, and gray lines represents control, +vincristine only, and +PAD2+vincristrine, respectively. Each point represents the leading edge of the signal at 15-min intervals, and data is presented as mean ± SEM. Thus, +PAD2+ vincristrine shows enhanced transport of signal compared to +vincristine only. **e** A specific lipid was loaded on one side of a neuron using microfluidic chamber and its transport in the presence of lidocaine. An identical setup had a PAD2 overexpressing neuron. Snapshots of transport between 0 and 75 min have been shown as indicated. The movement of granules (indicated by arrows) is significantly increased due to PAD2 expression even in the presence of transport blocker lidocaine. Schematic figure for the axon isolation chamber is in Online Resource 3

was stalled within 30 min of adding lidocaine or vincristine; however, transport was still active in the presence of overexpressed PAD2. These results suggest that deimination is involved in the regulation of specific cargo transport via specific molecular motors.

### The Effect of Deimination in Neuronal Transport in a Mouse Model

Next, we attempted to determine if pharmacological perturbations can relate deimination and neuronal transport to a functional visual (neuronal) outcome using an in vivo model system. Pattern electroretinograms (PERGs) primarily reflect the functional integrity of retinal ganglion cells (RGCs), including their signal transport and connectivity. Lidocaine can reduce PERG amplitude by blocking axonal retrotransport [32]. Here, we utilized a hybrid ND4(H), a cross between SLICK-H (genetically engineered mouse to express enhanced yellow fluorescent protein (EYFP) under regulation of the Thy1 promoter, rendering for a ready and easy visualization of dendrites (arbor) in a broad subset of neurons) [33] and ND4 (model for multiple sclerosis) mice [34, 35]. The hybrid ND4(H) mouse strain demonstrates the presence of the Thy1 marker in neuronal cells (Fig. 7d). To determine whether deimination would rescue transport under conditions where normal axonal transport is interrupted, we increased vector-mediated PAD2 expression in retinas. PERG measurement showed that PAD2 overexpression maintained up to 40% of baseline amplitude after lidocaine injection/inhibition and was significantly different from controls (without PAD2 overexpression) that lacked a visible wave (Fig. 7a–c). Western blots (Fig. 8a) showed increased expression of SNAP-25 in the eyes overexpressing PAD2 (Fig. 8c), suggesting that deimination facilitates the maintenance of the PERG wave by increasing neuronal transport. After 2 weeks, the eyes with PAD2 expression demonstrated stronger Thy1 signals compared to the control eyes (Fig. 7d, e).

## Discussion

There is growing recognition of the presence of quiescent neurons that are not being used in full capacity [36, 37], and their potential regenerative connectivity with targets in neighboring neurons which could allow them to be functionally restorative. Intuitively, increased transport should enhance protein biosynthesis, neurite growth, and connectivity, which are all hallmarks of neurodegeneration when they decrease. Graft experiments suggest that this can be reversed in the adult phase [3] and the evidence presented here suggests that normalization of deimination is one such regulatory mechanism to increase molecular transport, protein biosynthesis, and regenerative reconnectivity in lower vertebrates/amphibians (Fig. 1) and mammals (Figs. 1 and 7).

The intrinsic high rate of transport and translation underlie the maintenance of neural growth during development [38–40] which is substantially lost in adulthood, particularly in the CNS [6, 9, 12, 41, 42]. In adults, increased cargo transport and protein synthesis at the correct neuronal compartment/location are necessary for recovery from degeneration [41, 43, 44]. In contrast to the PNS, CNS neurons are restricted by the surrounding environment. Intrinsic regulation that increases the rate of transport and protein synthesis may overcome inhibition and result in functional restoration [3].

Long-term and irreversible PTMs, such as deimination [14], are important but underinvestigated regulators. In neuronal tissues, deimination shows a complexity of regulation in a cell-specific manner [17, 20]. Loss of deimination precedes the loss of visual function [21] and also modulates organelle mRNA transport [18]. We show here that increased and decreased deimination are associated with neuronal outgrowth (Fig. 1a) and retraction (Fig. 1d), respectively, suggesting that normalization of deimination levels may promote neurite outgrowth even in adults. Up- and downregulation of PAD2 affects REF deimination, distribution of REF-associated mRNAs, and timed cargo accumulation by molecular motors such as KIF21b and dynein/dynactin (Fig. 4c, e). The assembly of RNA granules and their transport are promoted by deimination from PAD2 overexpression (Figs. 3c and 4c, e). Conversely, downregulation of PAD2 using siRNA shows decreased neurite outgrowth (Fig. 2d) and that using shRNA against PAD2 shows decreased transport of mRNA cargo molecules (Fig. 4e). REF facilitates the delivery of specific mRNAs to their target cellular compartments to enhance local protein synthesis (Fig. 5), as depicted in our model shown in Fig. 8e. PAD2 overexpression resulted in increased cargo transport (Figs. 3a, b and 4e) that could overcome inhibition by the transport blockers lidocaine and vincristine (Fig. 6d, e). Normalization of deimination thus enhanced compartmental protein synthesis (Fig. 4b, c). Deimination-induced regenerative neurite outgrowth in adults (Fig. 1a, b) appeared to underlie functional visual restoration (Figs. 7 and 8). Neuronal trafficking and localized protein synthesis are highly regulated and intrinsic to neuronal activity [45]. We developed innovative fractionation methods to probe transported molecules in different neuronal compartments (Figs. 4, 5, and 6), and our techniques included using motor-associated, fluorophore-conjugated lipids as indicators of motor movement. Many neurodegenerative diseases such as glaucoma [46], Alzheimer's disease, and demyelinating diseases [47–49] are associated with

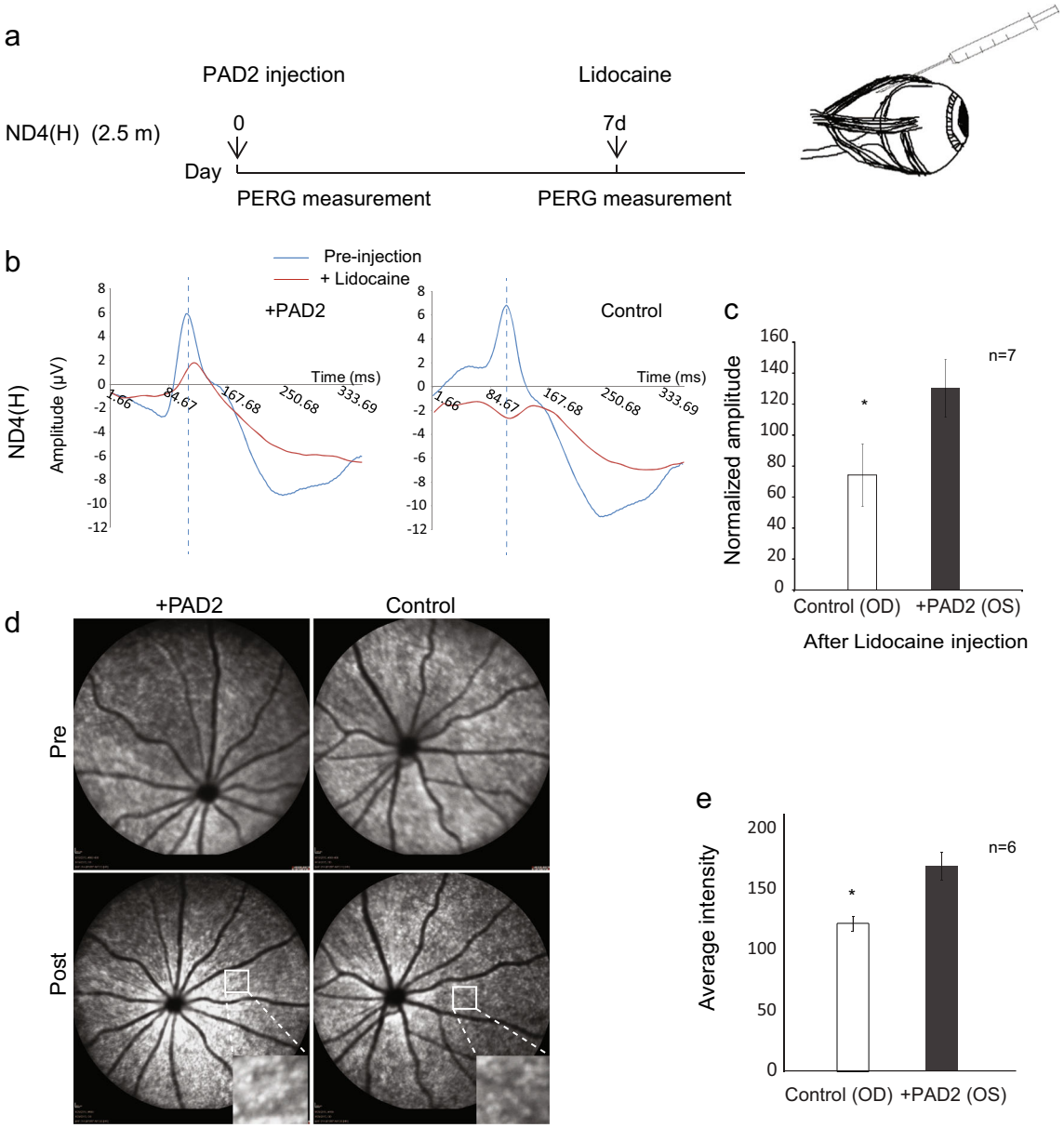


**Fig. 7** Modulation of deimination affects visual function. **a** Schematic depiction of a timeline experiment of pattern electroretinogram (PERG). PAD2 viral vector intravitreal injection and lidocaine retrobulbar injection (cartoon on the left) were performed as indicated. **b** Evaluation of PERG amplitudes in ND4(H) hybrid mice after 7 days of PAD2 overexpression in RGCs. Representative PERG signal from 2.5-month-old ND4(H) mice. The control and viral vector-mediated PAD2 expressing mice are as indicated. The pre- and post-lidocaine injection is shown in blue and red, respectively. PERG was measured 10 min after 4% lidocaine retrobulbar injection. Latency remains the same (dashed line) but amplitude changes. **c** Mean ± SEM for PERG amplitude normalized to baseline for PAD2-expressing (+PAD2) and control mice post-lidocaine injection (day 7th of PAD2 expression). ANOVA showed a significant difference between the control and treated groups ($n = 7$; $^*p < 0.005$). **d** Heidelberg optical coherence tomography imaging of RGC (Thy1) signal 1 week after PAD2 viral vector injection compared to control as indicated. Arrows indicate the Thy1-positive RGC cells. **e** Quantification of yellow fluorescent protein signal (Thy1) from comparative area (represented by boxed area in **d**) by ImageJ ($n = 6$;$^*p < 0.005$)

impaired axonal transport, the reversal of which may enhance neurite outgrowth [50] and lead to the restoration of visual function (Figs. 7 and 8). The proposed mechanism of deimination as one of the intrinsic regulators of recalibrating regenerative connectivity could be a new direction for functional restoration.

## Materials and Methods

### Animals

All animal protocols were approved by the Animal Care and Use Committee of the University of Miami or of the

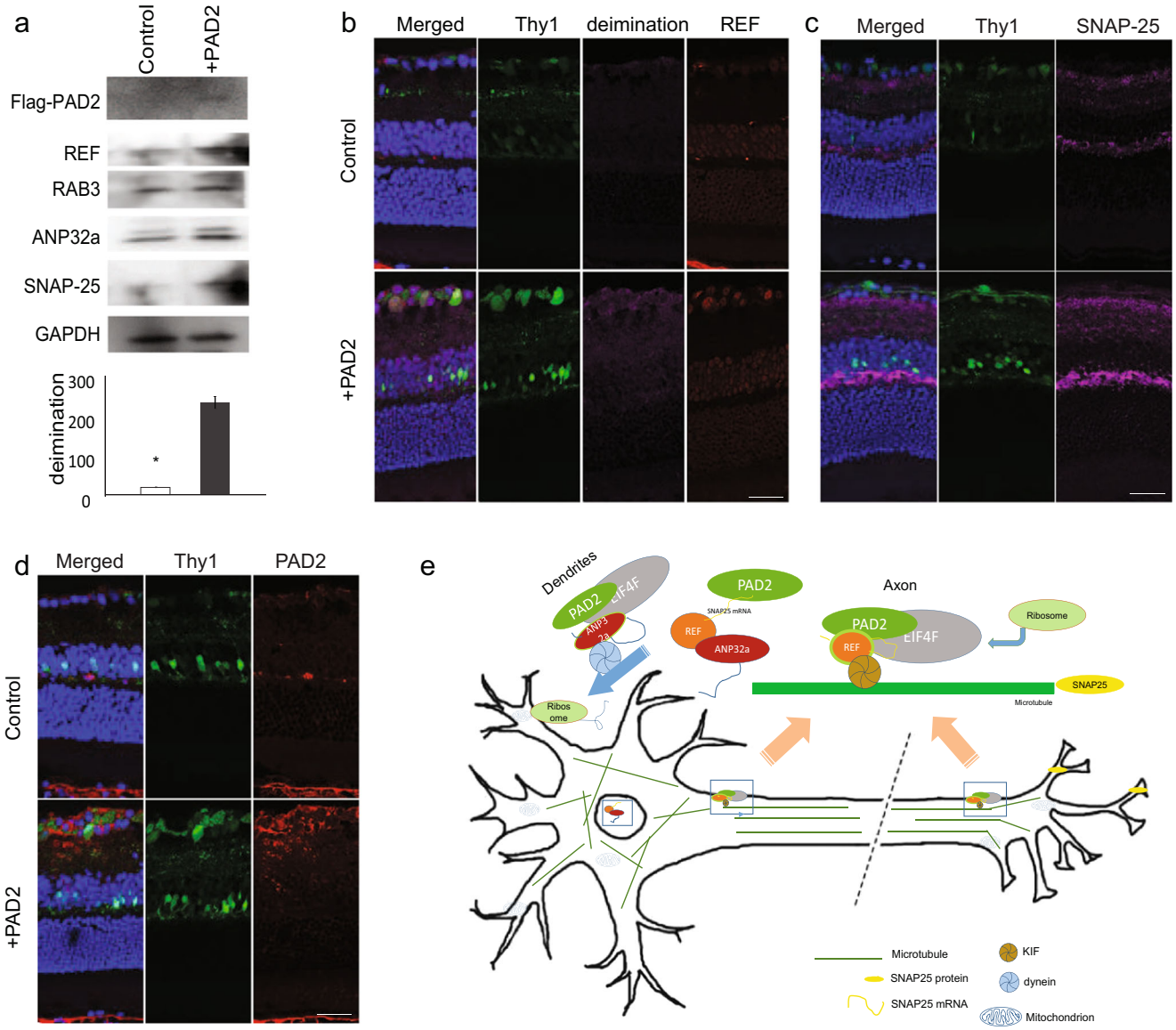


**Fig. 8** Modulation of deimination affects protein expression in vivo. **a** Representative Western blot of protein expression in PAD2-expressing (+PAD2) and control retinas ($n = 3$). Bottom panel is densitometric quantification of blots by ImageJ ($n = 3$; $^*p < 0.005$). **b**–**d** Representative IHC of Thy1, deimination, REF, SNAP-25, and PAD2 in PAD2-expressing (+PAD2) and control retina as indicated. Bar = 20 μm. The merged image with DAPI staining has been shown in the first panel. **e** Schematic diagram of deimination-mediated mRNA transport in neurons. REF and ANP32a are two mRNA-binding proteins that preferentially bind different mRNAs. They associate with each other in the soma and nucleus. When deiminated by PAD2 (indicated as green circle outline), the two proteins recruited the components of RNA granules such as eIFs and ribosomes and facilitated the mRNAs' (such SNAP-25, camk1) transport to different destinations

University at Buffalo. The original breeding pairs of ND4 mice were from The Hospital for Sick Children, Toronto, Canada, as a research gift, and a pathogen-free line was derived via embryo transfer performed at the Charles River Laboratory (Wilmington, MA). After confirmation of the genetic status, a colony was maintained at Bascom Palmer Eye Institute. Breeding pairs of SLICK mice were purchased from Jackson Lab (Bar Harbor, MA). Hybrids of ND4 mouse strains (ND4(H)) were derived from a cross between SLICK and ND4 mice. The sparse YFP labeling (Thy1-YFP) in these derivatives was confirmed by confocal scanning laser ophthalmoscopy (CSLO) imaging. All mice were maintained in the McKnight vivarium at the University of Miami.

## *Xenopus* Eye Rotation

*Xenopus laevis* tadpoles were obtained from Xenopus1, Dexter, MI. Nieuwkoop and Faber stage 56–57 tadpoles were anesthetized by immersion in 1:4000 MS-222 in 10% Holtfreter's solution [51]. The skin dorsal to the left

eye was opened with fine forceps, and the extraocular muscles were pinched apart. The eye was rotated 90° around the optic nerve. At 2 months postmetamorphosis, the frogs were anesthetized by subcutaneous injection with 1% MS-222 in 10% Holtfreter's solution, and the brains were fixed by immersion in 4% paraformaldehyde.

## Cell Culture

PC12 cells and Neuro 2A cells were purchased from ATCC (Manassas, VA). PC12 cells were grown in Dulbecco's modified Eagle's medium (DMEM, Cellgro, Manassas, VA), supplemented with 10% horse serum (ATCC) and 5% fetal bovine serum (Cellgro), and Neuron 2A cells were grown in DMEM (Cellgro), supplemented with 10% bovine serum (ATCC).

Primary cortical neuron-only cultures were prepared as previously described [52, 53] from the cortices of E18–19-day pups. The embryos were harvested through a cesarian section and the cortices rapidly dissected from the brain and placed in ice-cold HBSS. After removal of cerebral membranes, the cortices were enzymatically digested with 0.25% Trypsin-EDTA (Life Technologies) for 15 min at 37 °C. The resulting cellular suspension was filtered through a 70-μM filter and plated in MEM supplemented with 5% FBS, GlutaMax (Invitrogen/Life Technologies) and 15 mM glucose. The cells were plated on poly-D-lysine-coated coverslips at a density of 3000 cells/coverslip or on poly-D-lysine-coated 10-cm culture dish at a density of 50,000 cells.

## Virus Construct and PAD2 Expression in Animal Eyes

The Thy1 promoter region is located 2000 bp upstream of the Thy1 start codon. The sequence was identified using UCSC Genome Bioinformatics database. The BAC clone with the insert of genomic DNA covering this region was obtained from Children's Hospital Oakland Research Institute (CHORI). Primers (forward: 5′-AAAAAAACGCGTAA TCCAGTCCAGAAATGGGGGTG; reverse: 5′-GTGG GGGCTAGCGGACAAAGAAAACTGCACAATA) including restriction sites for *Mlu*1 and *Nhe*1 were prepared to amplify the region 0–2000 bp upstream of the Thy1 start codon. PCR products were subjected to verification by agarose gel electrophoresis. The PCR bands were excised and extracted from the agarose gel using a QIAGEN Gel Extraction Kit (Qiagen, Valencia, CA). The concentration of gel-purified DNA was determined using a UV/visible spectrophotometer. The insert and vector (pLionII) were simultaneously digested using restriction enzymes for excision of the CMV region on the vector. The digested inserts and pLionII were again subjected to gel electrophoresis and were extracted using the gel extraction kit. The vector was dephosphorylated with calf intestinal alkaline phosphatase (CIP). The digested vector and insert DNA were ligated in a ratio of 1:3 by incubating with T4 ligase at 37 °C for 2 h. The ligated constructs were used for transformation of TOP10 competent *E. coli* cells. The colonies of transformants were picked, and isolated DNA was confirmed for the presence of the insert by double digestion of the plasmid. The construct was further confirmed by DNA sequencing. The Thy1-containing pLionII was further subjected to digestion with *Pme*1 and *Not*1 restriction enzymes. PAD2 was amplified using the clone vector (Open Biosystem) with primers (forward: 5′-ATATAAGTTTAAACATGCTGCGCGAGCGGACCG; reverse 5′-TTTTGCGGCCGCTTACAGAGGAAAGC TGCTC) containing the *Pme*1 and *Not*1 restriction sites. PAD2 was ligated with the Thy1-pLionII vector using the same procedure as above.

## Virus Production and Transfection

Thy1-PAD2 pLionII and CMV-YFP pLionII constructs were transfected separately to human embryonic kidney (HEK-293) cells using FuGENE 6 Transfection Reagent (Roche). Briefly, structural vector (pCI-VSVG), envelope vector (pCPRΛEnv), and transfer vector (Thy1-PAD2 pLionII, empty pLionII vector with thy1 promoter only or CMV-YFP pLionII) were mixed in a 10:10:1 ratio; 21 μg of mixed DNA was incubated with 500 μL Opti-MEM (GIBCO) containing 5 μL FuGENE and mixed with HEK-293 cells. Media was changed every 3 days. Old media was collected and filtered with 0.4 μm Super Membrane (PALL). The filtered media was mixed with 100% PEG (polyethylene glycol 6000, USB Corporation, Solon, OH) using a 6:4 ratio (*v*/*v*) and centrifuged for 20 min at 3500 rpm at 4 °C. The pellet was resuspended in 300 μL DMEM; 10 μL of Thy1-PAD2 pLionII lentivirus was mixed with 1 μL of CMV-YFP pLionII lentivirus, and the whole mixture was added to HEK-293 cells. Neuronal cells were transfected using Lipofectamine™ 2000 (Invitrogen).

The siRNA experiments were performed using siRNA against PAD2 sequences [Stealth Select RNAi for rat (*Rattus norvegicus*) PAD2 (catalog numbers, Oligo id#, RSS309706, RSS309707, RSS309705). Control siRNA (Invitrogen) unrelated to any known mammalian sequence was also used. The siRNA was transfected using Lipofectamine 2000 (Invitrogen), following the manufacturer's instructions with minor modifications. Briefly, $10^6$ cells were collected for each transfection. All siRNAs used here were carefully evaluated and were found to downregulate PAD2 mRNA expression by about 60%. Cells were suspended in DMEM and plated onto 35-mm Petri dishes coated with poly-D-lysine (5 mg/mL) (Sigma Chemical Co., St. Louis, MO) after transfection and grown with differentiation medium containing 1% horse serum (ATCC) and 100 ng/mL NGF (Sigma Chemical Co.). The

cultures were maintained in a humidified atmosphere of 5% $CO_2$ at 37 °C. The medium was changed every 3 days.

## Ocular Injections

The mice were anesthetized with intraperitoneal ketamine (50 mg/kg) and xylazine (5 mg/kg). Retrobulbar injections of lidocaine (3 μL, 4%) were performed with a 23-gauge needle using a supraorbital approach [32]. Intravitreal injections were performed following established methods using a 5-μL Hamilton syringe with 30-gauge needle connecting to Ultra Micro Pump II (UMPII; World Precision Inc., Sarasota, FL) to deliver 0.5–1 μL viral construct. Reproducible injections are achieved by the UMPII device. An ointment containing antibiotics and gentamicin was applied to the injection site to prevent infection.

## Confocal Scanning Laser Ophthalmoscopy Imaging

The mice were anesthetized with intraperitoneal ketamine (50 mg/kg) and xylazine (5 mg/kg), and the eyes were dilated with 2.5% phenylephrine hydrochloride eye drops (Akorn, Lake Forest, IL) before imaging. A small drop of balanced salt solution (BSS, Alcon, Ft Worth, TX) was topically applied on the cornea to prevent dehydration when necessary. The mouse was placed on the platform and wrapped with paper tissue to keep body temperature. Each eye was imaged with a customized Heidelberg Engineering CSLO HRA II (Heidelberg Engineering, Heidelberg, Germany) at the wavelength for green fluorescence (488 nm) with a scan angle of 55° and scan rate of 51 frames per second.

## Pattern Electroretinogram Experiments and Flash Electroretinogram

ND4(H) mice aged 3–4 months were used in each batch of electrophysiological experiments. Briefly, the mice were anesthetized using ketamine and xylazine and were gently restrained with the use of a bite bar and a nose holder that allowed unobstructed vision. They were kept at a constant body temperature of 37 °C using a feedback-controlled heating pad with undilated pupils pointing laterally and upward. The active electrode (0.25 mm diameter silver wire configured to a semicircular loop of 2-mm radius) was placed on the corneal surface without limiting the field of view. Reference and ground electrodes were stainless steel needles inserted under the skin of the scalp and tail, respectively [54]. BSS (Alcon, Ft Worth, TX) was topically applied on the cornea to prevent dehydration for the duration of the recording. A visual stimulus of contrast-reversing horizontal bars (field area 50° × 58°, mean luminance 50 cd/m$^2$, spatial frequency 0.05 cycle/deg, contrast 98%, temporal frequency 1 Hz) was aligned with the projection of the pupil at the viewing distance of 15 cm. Eyes were not refracted for the viewing distance given that the mouse eye has a large depth of focus because of the pinhole pupil. Retinal signals were amplified (10,000-fold) and bandpass filtered (1–30 Hz). Three consecutive responses to each of 600 contrast reversals were recorded and were superimposed to check for consistency and then averaged (1800 sweeps). The PERG is a light-adapted response. To have a corresponding index of outer retinal function, a light-adapted flash electroretinogram (FERG) was also recorded with undilated pupils in response to strobe flashes of 20 cd/m$^2$/s superimposed on a steady background light of 12 cd/m$^2$ and presented within a Ganzfeld bowl. Averaged PERG and FERG consisting of a major positive wave followed by a slower negative wave were automatically analyzed to evaluate the response amplitude. This was defined as the sum of the absolute values of maximum and minimum voltages (peak-to-trough amplitude). Statistical analysis was performed by Student's $t$ test for unpaired data. $p < 0.05$ was considered statistically significant.

## Immunoprecipitation

All procedures were performed under RNase-free conditions for the following experiments. Neuron lysates prepared from rat brain were subjected to immunoprecipitation using different antibodies (Online Resource 1). Briefly, IP was carried out as follows: approximately 67 μg sepharose A beads suspended overnight in 200 μL of 50 mM sodium borate buffer pH 9.0 were incubated with 10 μg antibodies at room temperature for an hour. The beads and antibody were cross-linked by adding 10 μg dimethyl pimelimidate dihydrochloride (DMP) three times each with 2 h incubation at room temperature and then was kept at 4 °C overnight. Antibody-coupled beads were subsequently neutralized with 200 μL of 200 mM ethanolamine and washed with 1 mL of phosphate buffered saline (PBS) twice. The antibody-coupled beads were then incubated with 200 μg of cytosolic lysate for an hour at room temperature. The beads were washed twice with 500 μL of PBS and eluted with two 20 μL volumes of 100 mM glycine pH 3.0. The eluents were combined and divided into 2 equal amounts; one was kept at 4 °C for separation on SDS-PAGE and the other was used for mRNA isolation.

## Cloning, Purification, and In Vitro Deimination

REF clone (EMM1002-96824126) in plasmid pExpress1 procured from Open Biosystems (Huntsville, AL) was subcloned in pET19 vector (Novagen, Cat. No. 69677-3). The clone was sequenced and transformed in *E. coli* BL21 cells induced using 0.1 mM IPTG at absorbance values of 0.55–0.8 at 600 nm. Recombinant his-tagged REF was purified using two rounds of Ni-NTA column (Qiagen, Valencia, CA)

according to the protocol from the company. In the second round, the purified product from the first round was extensively dialyzed using a 3500 MWCO membrane (Sigma Chemical Co.) in PBS and repurified on a Ni-NTA column using 100 mM imidazole for elution. The final purified product was subjected to dialysis.

Briefly, PAD2 (Sigma-Aldrich, St. Louis, MO) was incubated under deiminating conditions with dialyzed REF. The recombinant REF (100 μg) was deiminated in vitro using 6 μg PAD2, repurified using a Ni-NTA column, dialyzed, and then quantified using Bradford's method.

IP experiments for the identification of translation complexes were performed using 5 μg of recombinant, his-tagged, deiminated and nondeiminated REF. Each batch was incubated with 1000 μg of cytosolic cell fraction extract for 1 h, incubated with approximately 50 μL of Ni-NTA beads, and loaded onto a mini column. The column was then washed with 50 volumes of binding buffer (PBS, 5 mM imidazole), and the bound his-tagged protein was eluted using 100 and 250 mM imidazole. Similar IPs were also performed with cultured RGC utilizing 5 μg of REF (deiminated and control) and 100 μg of protein extracts. Eluted proteins were either dialyzed to remove imidazole or acetone precipitated [55] and subjected to further analyses.

For protein identification, concentrated protein was digested in situ with sequencing grade trypsin (Promega Biosciences Inc., CA). Peptides were loaded onto 3 cm YMC ODS-A spherical 5–15 μm (YMC, Milford, MA) precolumns packed in-house in 360 × 100-μm fused silica and washed for 5 min to desalt prior to switching inline with the analytical column (7 cm YMC-ODS AQ spherical 5 μm particles packed in-house in 360 × 100-μm fused silica). Peptides were eluted along a 20-min gradient of 1–80% acetonitrile in 0.1% formic acid 0.1 M acetic acid into a Thermo Q-Exactive™ Orbitrap mass spectrometer fitted with a nanospray ionization source (Easy nLC 1000, Thermo Fisher Scientific). Spectra were collected in data-dependent mode with dynamic exclusion, selecting the top 5 most abundant ions for CID fragmentation. Peak lists were generated using Sequest (ThermoElectron, San Jose, CA) and submitted to a clustered version of the SequestHT search engine. Spectra were searched against SwissProt Fasta database (EBI, Cambridge, UK) with no more than two missed tryptic cleavages. Precursor ion tolerance was set to 10 ppm and 2 Da and fragment tolerance to 0.6 Da. Carbamidomethylation of cysteine was fixed for analysis; variable modifications of oxidized methionine and citrullinated arginine were permitted during the search. Sequest result files were loaded into Scaffold (Proteome Software, Portland, OR) for analysis through the PeptideProphet and ProteinProphet algorithms followed by manual validation of all proteins identified with at least two peptides and at a protein confidence of greater than 90%. For determination of deiminated/citrullinated peptides, the protein mixtures were subjected to chymotrypsin digestion and tandem mass spectrometry in an Orbitrap device (ThermoFinnigan, San Jose, CA).

## RNA Extraction and Reverse Transcription PCR

The eluents from IP as described above were collected, and RNA species together with REF or ANP32a were isolated using the miniRNA extraction kit (Stratagene Inc., La Jolla, CA) as per the manufacturer's recommended protocol. Total RNA was dissolved in DEPC-treated distilled water and converted to cDNA with the oligo dT (12–18) (Invitrogen Inc., Carlsbad, CA) following two-step reactions provided by the company. For detection of mRNA species, RT-PCR of IP product-derived mRNA was carried out with primers for different mRNAs (Online Resource 2) under a mild PCR condition according to the manufacturer's instruction (Advantage cDNA PCR kit; Clontech Inc., Mountain View, CA) and separated on a 2.0% agarose gel made with TBE buffer.

## Lectin Staining and Separations

Primary cortical neurons ($10^6$) were plated in the 10-cm plate for 6–7 days. The plate was washed 3x with PBS, and 10 mL PBS solution containing 2 μg/mL of lectin was added in the plates, which were maintained in a humidified atmosphere of 5% $CO_2$ at 37 °C for 4 h. Excess solution was then removed by a pipette and discarded. The plate was again washed 3x with PBS, and 40 μL of magnetic streptavidin beads (Thermo Fisher Scientific, Grand Island, NY) in 5 mL PBS were added to each flask and mixed on a shaker for 1 h. Excess solution was then removed. Using a plastic dish scraper, the cells were sheared and separated from the flask surface by force. The resulting liquid was transferred to a micropipette tube. A magnetic stand was used to separate beads with attached cellular particulate from the remaining solution. The supernatant was transferred to a separate container, and lectin 3 was added to make the final concentration 2 μg/mL. The remaining particulate was then washed once with 0.5 mL of 0.1% Tween-20 in PBS to remove any remaining buffer. For elution of particulate bound to the streptavidin beads, the beads were then washed with two aliquots of 50 μL elution buffer (0.1 M glycine at pH 2.0 for 5 min at 65 °C) followed by magnetic separation on each aliquot. Tris buffer pH 8.0 was added to 10% total volume for neutralization. The separation of the supernatant with lectin 3 was repeated, and the elution was collected as above.

## Neuron Growth in Axon Isolation Chamber and Ex Vivo/In Vitro Blocker

The slides were coated with 5 mg/mL poly-D-lysine (Sigma-Aldrich, St. Louis, MO) overnight and washed with distilled water. The axon isolation chamber (AXIS) (Millipore,

Temecula, CA) was attached to the slides as per the manufacturer's instructions. Briefly, neuronal cells (4 x $10^6$) were loaded into the channel area, and media was added into the wells (Online Resource 3). In order to overexpress the PAD2, we add 10 μL of Thy1-PAD2 pLionII lentivirus or the empty virus (control) to the channel areas 2 days after plating the neurons. The chambers were maintained in a humidified atmosphere of 5% $CO_2$ at 37 °C for 6 days. Growth media in chambers C and D (Online Resource 3) was replaced by media containing lipid (1 nM) and the blockers lidocaine (10 mM, Sigma-Aldrich, St. Louis, MO) or vincristine (50 nM, Sigma-Aldrich). 10 min after adding the blockers, and neuronal transport was analyzed using time-lapse microscopy (Carl Zeiss, Oberkochen, Germany). Images were acquired every 15 min for 3 h.

## Lipid Extraction and Mass Spectrometry Identification

IP samples were subjected to the Bligh and Dyer method [56] of lipid extraction with suitable modifications using butylated hydroxytoluene (Sigma-Aldrich, St. Louis, MO) and argon gas to prevent oxidation as per established procedures [57–59]. Briefly, the organic phase containing the extracted lipids was dried, flushed with argon gas, and stored at − 80 °C until mass spectrometric analysis. The corresponding aqueous phase was used for protein quantification using the Bradford protein assay as per established procedures [57].

Dried lipids were separated on an Ascentis Express column ($C_{18}$, 2.1 × 150 mm, 2.7 μm, 90 Å pore size, Sigma-Aldrich, St. Louis, MO) connected to an Easy nLC 1000 Liquid Chromatograph instrument (Thermo Fisher, San Jose, CA), which fed into a Q-Exactive orbitrap mass spectrometer (Thermo Fisher, San Jose, CA). A binary solvent system (mobile phase A consisted of acetonitrile:water (60:40) (*v*/*v*), 10 mM ammonium formate, and 0.1% formic acid; mobile phase B consisted of isopropanol: acetonitrile (90:10) (*v*/*v*), 10 mM ammonium formate, and 0.1% formic acid) was used in a 30-min gradient as per established methods [60, 61]. The following gradient conditions with increasing eluent B were used: 0–1.5 min increase to 32% B; 1.5–4 min increase to 45% B; 4–5 min increase to 52% B; 5–8 min increase to 58% B; 8–11 min increase to 66% B; 11–14 min increase to 70% B; 14–18 min increase to 75% B; 18–21 min increase to 97% B; 21–25 min held at 97% B; 25–25.1 min decrease to 32% B; and 25.1–30 min held at 32% B. Dried lipid samples were resuspended in 100 μL acetonitrile:isopropanol (50:50) (*v*/*v*), of which 2 μL were injected. Flow rate was set to 400 μL/min. The Q-Exactive mass spectrometer equipped with a HESI-I probe was set for positive mode acquisition. The method for lipid analysis was based on previously optimized and experimentally determined parameters [62]. Mass resolution was set to 70,000 for full-MS with Top-10 $MS^2$ at resolution 17,500 (FWHM at *m*/*z* 200 for both). Normalized collision energy was set to 35. A dynamic exclusion of 8 s was found to resolve partially separated isomers. An isolation window of 1.2 Da was found to be the optimal balance between a good ion transmission and false positive IDs by the LipidSearch 4.0 (Thermo Fisher, San Jose, CA). An injection time of 75 ms was found as optimal. An exclusion list was determined by injecting blank resuspension buffer under the same conditions and was added to the method above. Spray voltage was set to 3000 V, the ion transfer tube was held at 285 °C, S-Lens was set to 45%, and sheath gas and auxiliary gas were held at 60 and 20 arbitrary units, respectively. Sweep gas was at 1 arbitrary unit. The automatic gain control (AGC) of full-MS was 1e6, and for $MS^2$ at 1e5. Mass range was 150–2000 *m*/*z*, with a first fixed mass at 75 Da [62].

## Virus Construct

The full-length mRNA sequences of Synaptosomal-associated protein 25 (Snap25) (NM_011428.3), Syntaxin binding protein 3 (Stxbp3) (NM_011504.1), and Sphingosine kinase 2 transcript variant 1 (Sphk2) (NM_203280.3) were obtained from NCBI as referred. The cDNAs generated from the total mouse brain mRNAs by reverse transcription using oligo dT.

The 5′ UTR region is defined by full-sequence mRNAs upstream of start codon (AUG), and 3′ UTR is defined by the downstream of the stop codon (UAA or UAG). Different sets of primers including restriction sites for *Bam*HI (forward) and *Nde*1 (reverse) were prepared to amplify the 5′ UTR of Sphk2 (464 bp) and SNAP-25 (225 bp). mCherry was cloned from pmCherry vector using primers including restriction sites for *Nde*1 (forward) and *Not*1 (reverse). For Stxbp3, the 5′ UTR sequence was included in the primers. The 5′ UTR and mCherry were cloned together by PCR using the primers including restriction sites for *Bam*HI (forward) and *Not*I (reverse). Another set of primers including restriction sites for *Not*I (forward) and *Kpn*I (reverse) is designed to clone 3′ UTR region of Sphk2 (1286 bp), SNAP-25 (1316 bp), and Stxbp3 (617 bp). A summary of all the primers is listed in Online Resource 2. PCR products were subjected to verification by agarose gel electrophoresis. The PCR bands were excised and extracted from the agarose gel using a QIAGEN Gel Extraction Kit (Qiagen, Valencia, CA). The concentration of gel-purified DNA was determined using a UV/visible spectrophotometer. The inserts and vector pWPXL (Addgene) were simultaneously digested using restriction enzymes which would excise the GFP region on the vector. The digested inserts and vector were again subjected to gel electrophoresis and were extracted using the Gel Extraction Kit. The vector was dephosphorylated with CIP. The digested vector and insert DNA were ligated in a ratio of 1:3 by incubating with T4 ligase at 37 °C for 2 h. The ligated constructs were used for transformation of DH5α competent *E. coli* cells. The colonies

of transformants were picked and isolated DNA was subjected to confirmation for the presence of insert by double digestion of the plasmid and also by the expression of mCherry. The construct was further confirmed by DNA sequencing.

## Virus Production and Transfection

pWPXL constructs were transfected separately to HEK-293 cells using FuGENE 6 Transfection Reagent (Roche—Cat. No. 11815091001). Briefly, structural vector (psPAX2), envelope vector (pMD2.G), and transfer vector (pWPXL-stxbp3/sphk2/snap25) were mixed with 10:10:1 ratio; 21 μg of mixed DNA was incubated with 500 μL Opti-MEM (GIBCO) containing 5 μL FuGENE and mixed with HEK-293 cells. Media was changed every 3 days. Old media was collected and filtrated with 0.4 μm Super Membrane (PALL). The viral construct containing REF-GFP or ANP32a-GFP was purchased from Genecopeoia (EX-Mm34605-lv122; EX-Mm01200-Lv103). The virus was produced in HEK-293 cell following the procedures provided in the Lenti-Pac™ Lentiviral Packaging Systems kit (HPK-LvTR-20).

The 2-day primary cortical neurons were co-infected with REF-GFP or ANP32a-GFP and one of the viruses containing the construct (Snap25, Stxbp3, or Sphk2) (*v*/*v* 1:1) by replacing one third of the medium with the media containing the virus. The neurons which without overexpression of REF-GFP or ANP32a-GFP were used as controls. The expression of the proteins was confirmed after 24–48 h. Imaging was performed after 48 h.

## Microscopy

Fluorescence recovery after photobleaching (FRAP) was done using Leica SP8 (Mannheim, Germany) utilizing a 63x Plan Apo (1.4 NA). First, an appropriate field was localized that expressed both endogenous markers. Next, the nuclear region of interest was selected for the cell. Prephotobleach images were acquired using the appropriate laser and filter setting. GFP detection was accomplished using a 488 nm excitation laser, and a 490–532 nm emission. mCherry was detected using a 561 laser and a 577–680-nm emission. Photobleaching then commenced with a 561-nm laser for 60 s. Finally, recovery images were acquired at a rate of one image per minute for a total duration of 10 min.

## Quantification, Bioinformatics Identification, and Statistical Analysis

Chromatograms were automatically processed using LipidSearch 4.0, with a precursor mass tolerance of 3 ppm, a product mass tolerance of 7 ppm, and an m-score threshold of 3 as per established methods [62]. An internal standard was used for ratiometric quantification in a two-step process [63, 64]. Briefly, in the first step, the most abundant lipids in the class were quantified using internal standards, and the measurements from the first step were used for quantification of low-abundance species in the second step [57, 64, 65]. The internal standards were procured from and made by Avanti Polar Lipids (Alabaster, AL) in conjunction with LipidMaps (www.lipidmaps.org) specifically for LC-MS quantification use. The following were used in ratiometric quantification of phospholipids: 17:0–20:4 PI (catalog no. LM-1502) for PI, 17:0–20:4 PS (catalog no. LM-1302) for PS, 17:0–20:4 PE (catalog no. LM-1102) for PE, and 17:0–20:4 PC (catalog no. LM-1002) for PC. The lipid amount was normalized to the protein amount determined from the corresponding aqueous phase as described above. Lipids were also subjected to normalization as a percent of total lipids. Comparison of lipid profiles between tissues or fluids was performed using in-house written Excel macros as described previously for other studies [57, 59, 63, 65]. Reported lipids were found statistically significant using Student's *t* test ($p \leq 0.05$). For lipids that were unique, a value of 0 was used for the groups devoid of the specific lipid. The number of samples was then assumed to be equivalent to the frequency of occurrence of the unique group. The select common lipid species had statistically significant differences between two groups by ANOVA. Scheffe's post hoc test showed that select lipid species in the control group were statistically different from the comparison group ($p \leq 0.05$).

**Acknowledgments** We thank A. Trzeciecka for providing part of the neurons. We thank G. Gaidosh for assistance with microscopy. We thank Dr. K. Park for the critical comments on the manuscript.

**Funding Information** This work was partially supported by an unrestricted grant from Research to Prevent Blindness to the University of Miami, DoD grant W81XWH-16-1-0715, and NIH grants P30 EY014801, EY014957, EY019077, NS034773, and U01EY027257.

## Compliance with Ethical Standards

**Conflict of Interest** The authors declare that they have no conflict of interest.

## References

1. Martin KC, Ephrussi A (2009) mRNA localization: gene expression in the spatial dimension. Cell 136(4):719–730. https://doi.org/10.1016/j.cell.2009.01.044
2. Kim S, Martin KC (2015) Neuron-wide RNA transport combines with netrin-mediated local translation to spatially regulate the synaptic proteome. eLife 4:4. https://doi.org/10.7554/eLife.04158

3. Kalinski AL, Sachdeva R, Gomes C, Lee SJ, Shah Z, Houle JD, Twiss JL (2015) mRNAs and protein synthetic machinery localize into regenerating spinal cord axons when they are provided a substrate that supports growth. J Neurosci 35(28):10357–10370. https://doi.org/10.1523/JNEUROSCI.1249-15.2015
4. Park KK, Liu K, Hu Y, Smith PD, Wang C, Cai B, Xu B, Connolly L et al (2008) Promoting axon regeneration in the adult CNS by modulation of the PTEN/mTOR pathway. Science 322(5903):963–966. https://doi.org/10.1126/science.1161566
5. Sun F, Park KK, Belin S, Wang D, Lu T, Chen G, Zhang K, Yeung C et al (2011) Sustained axon regeneration induced by co-deletion of PTEN and SOCS3. Nature 480(7377):372–375. https://doi.org/10.1038/nature10594
6. Steward O, Levy WB (1982) Preferential localization of polyribosomes under the base of dendritic spines in granule cells of the dentate gyrus. J Neurosci 2(3):284–291
7. Kar AN, MacGibeny MA, Gervasi NM, Gioio AE, Kaplan BB (2013) Intra-axonal synthesis of eukaryotic translation initiation factors regulates local protein synthesis and axon growth in rat sympathetic neurons. J Neurosci 33(17):7165–7174. https://doi.org/10.1523/JNEUROSCI.2040-12.2013
8. Friede RL, Bischhausen R (1980) The fine structure of stumps of transected nerve fibers in subserial sections. J Neurol Sci 44(2–3):181–203
9. Han SB, Kim H, Skuba A, Tessler A, Ferguson T, Son YJ (2012) Sensory axon regeneration: a review from an in vivo imaging perspective. Experimental Neurobiology 21(3):83–93. https://doi.org/10.5607/en.2012.21.3.83
10. Liuzzi FJ, Tedeschi B (1991) Peripheral nerve regeneration. Neurosurg Clin N Am 2(1):31–42
11. Windle WF (1980) Inhibition of regeneration of severed axons in the spinal cord. Exp Neurol 69(1):209–211
12. Erturk A, Hellal F, Enes J, Bradke F (2007) Disorganized microtubules underlie the formation of retraction bulbs and the failure of axonal regeneration. J Neurosci 27(34):9169–9180. https://doi.org/10.1523/JNEUROSCI.0612-07.2007
13. Verma P, Chierzi S, Codd AM, Campbell DS, Meyer RL, Holt CE, Fawcett JW (2005) Axonal protein synthesis and degradation are necessary for efficient growth cone regeneration. J Neurosci 25(2):331–342. https://doi.org/10.1523/JNEUROSCI.3073-04.2005
14. Vossenaar ER, Zendman AJ, van Venrooij WJ, Pruijn GJ (2003) PAD, a growing family of citrullinating enzymes: genes, features and involvement in disease. Bioessays 25(11):1106–1118. https://doi.org/10.1002/bies.10357
15. Bhattacharya SK, Crabb JS, Bonilha VL, Gu X, Takahara H, Crabb JW (2006) Proteomics implicates peptidyl arginine deiminase 2 and optic nerve citrullination in glaucoma pathogenesis. Invest Ophthalmol Vis Sci 47(6):2508–2514
16. Enriquez-Algeciras M, Ding D, Chou TH, Wang J, Padgett KR, Porciatti V, Bhattacharya SK (2011) Evaluation of a transgenic mice model of multiple sclerosis with non invasive methods. Invest Ophthalmol Vis Sci 52:2405–2411
17. Bhattacharya SK (2009) Retinal deimination in aging and disease. IUBMB Life 61(5):504–509
18. Ding D, Enriquez-Algeciras M, Dave KR, Perez-Pinzon M, Bhattacharya SK (2012) The role of deimination in ATP5b mRNA transport in a transgenic mouse model of multiple sclerosis. EMBO Rep 13(3):230–236
19. Moscarello MA, Wood DD, Ackerley C, Boulias C (1994) Myelin in multiple sclerosis is developmentally immature. J Clin Invest 94(1):146–154
20. Bhattacharya SK, Sinicrope B, Rayborn ME, Hollyfield JG, Bonilha VL (2008) Age-related reduction in retinal deimination levels in the F344BN rat. Aging Cell 7(3):441–444. https://doi.org/10.1111/j.1474-9726.2008.00376.x
21. Enriquez-Algeciras M, Ding D, Mastronardi FG, Marc RE, Porciatti V, Bhattacharya SK (2013) Deimination restores inner retinal visual function in murine demyelinating disease. J Clin Invest 123(2):646–656
22. Udin SB (2005) Chronic melatonin and binocular plasticity in Xenopus frogs. Gen Comp Endocrinol 142(3):274–279. https://doi.org/10.1016/j.ygcen.2005.01.014
23. Udin SB, Fisher MD (1985) The development of the nucleus isthmi in Xenopus laevis. I. Cell genesis and the formation of connections with the tectum. J Comparative Neurology 232(1):25–35. https://doi.org/10.1002/cne.902320103
24. Sim ME, Lyoo IK, Streeter CC, Covell J, Sarid-Segal O, Ciraulo DA, Kim MJ, Kaufman MJ et al (2007) Cerebellar gray matter volume correlates with duration of cocaine use in cocaine-dependent subjects. Neuropsychopharmacology: Official Publication Am College Neuropsychopharmacology 32(10):2229–2237. https://doi.org/10.1038/sj.npp.1301346
25. Herold A, Suyama M, Rodrigues JP, Braun IC, Kutay U, Carmo-Fonseca M, Bork P, Izaurralde E (2000) TAP (NXF1) belongs to a multigene family of putative RNA export factors with a conserved modular architecture. Mol Cell Biol 20(23):8996–9008
26. Khan MZ, Vaidya A, Meucci O (2011) CXCL12-mediated regulation of ANP32A/Lanp, a component of the inhibitor of histone acetyl transferase (INHAT) complex, in cortical neurons. J Neuroimmune Pharmacology : Official J Soc NeuroImmune Pharmacology 6(1):163–170. https://doi.org/10.1007/s11481-010-9228-5
27. Cohen MS, Bas Orth C, Kim HJ, Jeon NL, Jaffrey SR (2011) Neurotrophin-mediated dendrite-to-nucleus signaling revealed by microfluidic compartmentalization of dendrites. Proc Natl Acad Sci U S A 108(27):11246–11251. https://doi.org/10.1073/pnas.1012401108
28. Corral-Debrinski M (2007) mRNA specific subcellular localization represents a crucial step for fine-tuning of gene expression in mammalian cells. Biochim Biophys Acta 1773(4):473–475
29. Shigeoka T, Jung H, Jung J, Turner-Bridger B, Ohk J, Lin JQ, Amieux PS, Holt CE (2016) Dynamic axonal translation in developing and mature visual circuits. Cell 166(1):181–192. https://doi.org/10.1016/j.cell.2016.05.029
30. Kanai A, Hiruma H, Katakura T, Sase S, Kawakami T, Hoka S (2001) Low-concentration lidocaine rapidly inhibits axonal transport in cultured mouse dorsal root ganglion neurons. Anesthesiology 95(3):675–680
31. LaPointe NE, Morfini G, Brady ST, Feinstein SC, Wilson L, Jordan MA (2013) Effects of eribulin, vincristine, paclitaxel and ixabepilone on fast axonal transport and kinesin-1 driven microtubule gliding: implications for chemotherapy-induced peripheral neuropathy. Neurotoxicology 37:231–239. https://doi.org/10.1016/j.neuro.2013.05.008
32. Chou TH, Park KK, Luo X, Porciatti V (2013) Retrograde signaling in the optic nerve is necessary for electrical responsiveness of retinal ganglion cells. Invest Ophthalmol Vis Sci 54(2):1236–1243. https://doi.org/10.1167/iovs.12-11188
33. Young P, Qiu L, Wang D, Zhao S, Gross J, Feng G (2008) Single-neuron labeling with inducible Cre-mediated knockout in transgenic mice. Nat Neurosci 11(6):721–728. https://doi.org/10.1038/nn.2118
34. Mastronardi FG, Ackerley CA, Arsenault L, Roots BI, Moscarello MA (1993) Demyelination in a transgenic mouse: a model for multiple sclerosis. J Neurosci Res 36(3):315–324. https://doi.org/10.1002/jnr.490360309
35. Johnson RS, Roder JC, Riordan JR (1995) Over-expression of the DM-20 myelin proteolipid causes central nervous system demyelination in transgenic mice. J Neurochem 64(3):967–976

36. Ahn S, Joyner AL (2005) In vivo analysis of quiescent adult neural stem cells responding to Sonic hedgehog. Nature 437(7060):894–897
37. Song J, Zhong C, Bonaguidi MA, Sun GJ, Hsu D, Gu Y, Meletis K, Huang ZJ et al (2012) Neuronal circuitry mechanism regulating adult quiescent neural stem-cell fate decision. Nature 489(7414): 150–154
38. Bassell GJ, Kelic S (2004) Binding proteins for mRNA localization and local translation, and their dysfunction in genetic neurological disease. Curr Opin Neurobiol 14(5):574–581. https://doi.org/10.1016/j.conb.2004.08.010
39. Bassell GJ, Zhang H, Byrd AL, Femino AM, Singer RH, Taneja KL, Lifshitz LM, Herman IM et al (1998) Sorting of beta-actin mRNA and protein to neurites and growth cones in culture. J Neurosci 18(1):251–265
40. Besse F, Ephrussi A (2008) Translational control of localized mRNAs: restricting protein synthesis in space and time. Nat Rev Mol Cell Biol 9(12):971–980. https://doi.org/10.1038/nrm2548
41. Doron-Mandel E, Fainzilber M, Terenzio M (2015) Growth control mechanisms in neuronal regeneration. FEBS Lett 589(14):1669–1677. https://doi.org/10.1016/j.febslet.2015.04.046
42. Liu K, Tedeschi A, Park KK, He Z (2011) Neuronal intrinsic mechanisms of axon regeneration. Annu Rev Neurosci 34:131–152
43. Yoo S, van Niekerk EA, Merianda TT, Twiss JL (2010) Dynamics of axonal mRNA transport and implications for peripheral nerve regeneration. Exp Neurol 223(1):19–27. https://doi.org/10.1016/j.expneurol.2009.08.011
44. Benowitz LI, Yin Y (2007) Combinatorial treatments for promoting axon regeneration in the CNS: strategies for overcoming inhibitory signals and activating neurons' intrinsic growth state. Dev Neurobiol 67(9):1148–1165. https://doi.org/10.1002/dneu.20515
45. Encalada SE, Goldstein LS (2014) Biophysical challenges to axonal transport: motor-cargo deficiencies and neurodegeneration. Annu Rev Biophys 43:141–169. https://doi.org/10.1146/annurev-biophys-051013-022746
46. Crish SD, Sappington RM, Inman DM, Horner PJ, Calkins DJ (2010) Distal axonopathy with structural persistence in glaucomatous neurodegeneration. Proc Natl Acad Sci U S A 107(11):5196–5201. https://doi.org/10.1073/pnas.0913141107
47. LaPointe NE, Morfini G, Pigino G, Gaisina IN, Kozikowski AP, Binder LI, Brady ST (2009) The amino terminus of tau inhibits kinesin-dependent axonal transport: implications for filament toxicity. J Neurosci Res 87(2):440–451. https://doi.org/10.1002/jnr.21850
48. Koch JC, Bitow F, Haack J, d'Hedouville Z, Zhang JN, Tonges L, Michel U, Oliveira LM et al (2015) Alpha-synuclein affects neurite morphology, autophagy, vesicle transport and axonal degeneration in CNS neurons. Cell Death Dis 6:e1811. https://doi.org/10.1038/cddis.2015.169
49. Roy S, Zhang B, Lee VM, Trojanowski JQ (2005) Axonal transport defects: a common theme in neurodegenerative diseases. Acta Neuropathol 109(1):5–13. https://doi.org/10.1007/s00401-004-0952-x
50. Winans AM, Collins SR, Meyer T (2016) Waves of actin and microtubule polymerization drive microtubule-based transport and neurite growth before single axon formation. eLife 5:5. https://doi.org/10.7554/eLife.12387
51. Nieuwkoop PD, Faber J (1967) A normal table of *Xenopus laevis* (Daudin). 2nd edn. North-Holland Publishing Company, Amsterdam
52. Kim EJ, Raval AP, Perez-Pinzon MA (2008) Preconditioning mediated by sublethal oxygen-glucose deprivation-induced cyclooxygenase-2 expression via the signal transducers and activators of transcription 3 phosphorylation. J Cereb Blood Flow Metab 28(7):1329–1340. https://doi.org/10.1038/jcbfm.2008.26
53. Thompson JW, Dave KR, Saul I, Narayanan SV, Perez-Pinzon MA (2013) Epsilon PKC increases brain mitochondrial SIRT1 protein levels via heat shock protein 90 following ischemic preconditioning in rats. PLoS One 8(9):e75753. https://doi.org/10.1371/journal.pone.0075753
54. Porciatti V (2007) The mouse pattern electroretinogram. Doc Ophthalmol 115(3):145–153. https://doi.org/10.1007/s10633-007-9059-8
55. Patel N, Solanki E, Picciani R, Cavett V, Caldwell-Busby JA, Bhattacharya SK (2008) Strategies to recover proteins from ocular tissues for proteomics. Proteomics 8(5):1055–1070
56. Bligh EG, Dyer WJ (1959) A rapid method of total lipid extraction and purification. Can J Biochem Physiol 37(8):911–917
57. Aribindi K, Guerra Y, Lee RK, Bhattacharya SK (2013) Comparative phospholipid profiles of control and glaucomatous human trabecular meshwork. Invest Ophthalmol Vis Sci 54(4): 3037–3044
58. Crane AM, Hua HU, Coggin AD, Gugiu BG, Lam BL, Bhattacharya SK (2012) Mass spectrometric analyses of phosphatidylcholines in alkali-exposed corneal tissue. Invest Ophthalmol Vis Sci 53(11):7122–7130
59. Aribindi K, Guerra Y, Piqueras Mdel C, Banta JT, Lee RK, Bhattacharya SK (2013) Cholesterol and glycosphingolipids of human trabecular meshwork and aqueous humor: comparative profiles from control and glaucomatous donors. Curr Eye Res 38(10): 1017–1026
60. Bird SS, Marur VR, Sniatynski MJ, Greenberg HK, Kristal BS (2011) Lipidomics profiling by high-resolution LC-MS and high-energy collisional dissociation fragmentation: focus on characterization of mitochondrial cardiolipins and monolysocardiolipins. Anal Chem 83(3):940–949. https://doi.org/10.1021/ac102598u
61. Hu C, van Dommelen J, van der Heijden R, Spijksma G, Reijmers TH, Wang M, Slee E, Lu X et al (2008) RPLC-ion-trap-FTMS method for lipid profiling of plasma: method validation and application to p53 mutant mouse model. J Proteome Res 7(11):4982–4991. https://doi.org/10.1021/pr800373m
62. Josef Ruzicka, Kevin J. McHale, David Peake (2014) Data acquisition parameters optimization of quadrupole orbitrap for global lipidomics on LC-MS/MS time frame. Paper presented at the American Society for Mass Spectrometry, Baltimore, Maryland
63. Edwards G, Aribindi K, Guerra Y, Lee RK, Bhattacharya SK (2014) Phospholipid profiles of control and glaucomatous human aqueous humor. Biochimie 101:232–247. https://doi.org/10.1016/j.biochi.2014.01.020
64. Yang K, Zhao Z, Gross RW, Han X (2009) Systematic analysis of choline-containing phospholipids using multi-dimensional mass spectrometry-based shotgun lipidomics. J Chromatogr B Analyt Technol Biomed Life Sci 877(26):2924–2936
65. Edwards G, Aribindi K, Guerra Y, Bhattacharya SK (2014) Sphingolipids and ceramides of mouse aqueous humor: comparative profiles from normotensive and hypertensive DBA/2J mice. Biochimie 105:99–109. https://doi.org/10.1016/j.biochi.2014.06.019

## Affiliations

Di Ding[1,2] · Mabel Enriquez-Algeciras[1,2] · Anddre Osmar Valdivia[1,2] · Juan Torres[1,2] · Cameron Pole[2] · John W Thompson[3] · Tsung-han Chou[1,2] · Miguel Perez-Pinzon[2,4] · Vittorio Porciatti[1,2] · Susan Udin[5] · Eric Nestler[6] · Sanjoy K. Bhattacharya[1,2]

[1] Bascom Palmer Eye Institute, University of Miami, 1638 N.W. 10th Avenue, #706, Miami, FL 33136, USA

[2] Department of Ophthalmology/Neuroscience Program, University of Miami, Miami, FL 33136, USA

[3] Neurological Surgery, University of Miami, Miami, FL 33136, USA

[4] Department of Neurology, University of Miami, Miami, FL 33136, USA

[5] Department of Physiology and Biophysics, State University of New York, Buffalo, 553 Biomedical Res. Building, Buffalo, NY 14214, USA

[6] Fishberg Department of Neuroscience and Friedman Brain Institute, Icahn School of Medicine at Mount Sinai, One Gustave L. Levy Place, Box 1065, New York, NY 10029, USA